JEM Journal of Experimental Medicine

ARTICLE

SARS-CoV-2 infection and recovery in children: Distinct T cell responses in MIS-C compared to COVID-19

Ksenia Rybkina[1], Joseph N. Bell[2], Marissa C. Bradley[2], Teddy Wohlbold[2], Marika Scafuro[2], Wenzhao Meng[3], Rebecca C. Korenberg[2], Julia Davis-Porada[1], Brett R. Anderson[2], Rachel J. Weller[2], Joshua D. Milner[2], Anne Moscona[1,2], Matteo Porotto[2], Eline T. Luning Prak[3], Kalpana Pethe[2], Thomas J. Connors[2], and Donna L. Farber[1,4]

SARS-CoV-2 infection for most children results in mild or minimal symptoms, though in rare cases severe disease can develop, including a multisystem inflammatory syndrome (MIS-C) with myocarditis. Here, we present longitudinal profiling of immune responses during acute disease and following recovery in children who developed MIS-C, relative to children who experienced more typical symptoms of COVID-19. T cells in acute MIS-C exhibited transient signatures of activation, inflammation, and tissue residency which correlated with cardiac disease severity, while T cells in acute COVID-19 upregulated markers of follicular helper T cells for promoting antibody production. The resultant memory immune response in recovery showed increased frequencies of virus-specific memory T cells with pro-inflammatory functions in children with prior MIS-C compared to COVID-19 while both cohorts generated comparable antibody responses. Together our results reveal distinct effector and memory T cell responses in pediatric SARS-CoV-2 infection delineated by clinical syndrome, and a potential role for tissue-derived T cells in the immune pathology of systemic disease.

Introduction

Children have decreased susceptibility and greater resiliency to SARS-CoV-2 infection relative to adults, who are at much higher risk for severe disease, prolonged symptoms, and mortality (Lu et al., 2020; Parri et al., 2020). However, in rare instances, children can manifest severe disease requiring hospitalization. Notably, in spring 2020, a newly identified multisystem inflammatory syndrome in children (MIS-C) presented weeks after SARS-CoV-2 infection and was marked by systemic inflammation, autoimmunity, and myocarditis (Cheung et al., 2020; Riphagen et al., 2020; Verdoni et al., 2020). Children can also develop respiratory symptoms similar to COVID-19 in adults, which has become more prevalent among the pediatric population in recent infection waves (Cloete et al., 2022; Martin et al., 2022; Wang et al., 2022). Understanding the immune processes associated with different outcomes of pediatric SARS-CoV-2 infection and the resultant establishment of long-term protective immunity are important for developing prevention and treatment strategies.

There have been many studies on the acute clinical and immunological manifestations of MIS-C. Hallmarks of disease include multi-organ involvement, most notably cardiac dysfunction in the setting of high levels of circulating proinflammatory cytokines, similar to those seen in toxic shock syndrome, and the presence of autoantibodies (Carter et al., 2020; Gruber et al., 2020). While MIS-C was originally thought to resemble Kawasaki disease, an inflammatory syndrome associated with vasculitis and heart disease in young children, MIS-C patients were found to exhibit immune and inflammatory profiles more closely resembling macrophage activation syndromes (Rodriguez-Smith et al., 2021; Sacco et al., 2022; Sharma et al., 2021). Additionally, the high incidence of gastrointestinal symptoms during the acute phase of MIS-C (Cheung et al., 2020; Feldstein et al., 2020) suggests a distinct pathophysiologic spectrum in MIS-C. The successful treatment of MIS-C with intravenous immunoglobulin (IVIG) and steroids further implicates systemic immune dysregulation in disease pathogenesis (Belhadjer et al., 2020; Crosby et al., 2021). While circulating autoantibodies reactive to endothelial cell components may account for the cardiovascular dysfunction in acute

[1]Department of Microbiology and Immunology, Columbia University Irving Medical Center, New York, NY, USA; [2]Department of Pediatrics, Columbia University Vagelos College of Physicians and Surgeons, New York, NY, USA; [3]Department of Pathology and Laboratory Medicine, Perelman School of Medicine, University of Pennsylvania, Philadelphia, PA, USA; [4]Department of Surgery, Columbia Irving University Medical Center, New York, NY, USA.

Correspondence to Donna L. Farber: df2396@cumc.columbia.edu; Thomas J. Connors: tc2625@cumc.columbia.edu.

MIS-C (Burbelo et al., 2022; Porritt et al., 2021a; Ramaswamy et al., 2021), the underlying mechanisms for mucosal tissue damage remain unclear. It is also not known whether the systemic inflammation observed in MIS-C is induced by SARS-CoV-2 infection or secondary effects of immune activation and/or tissue damage.

There is evidence for a primary role for T cells in mediating immune dysfunction in MIS-C. Studies by Arditi and others identified preferential expansion of T cells expressing specific TCR Vβ chains in a significant proportion (50–75%) of acute MIS-C patients, suggesting superantigen-like T cell activation through direct TCR binding (Moreews et al., 2021; Noval Rivas et al., 2021; Porritt et al., 2021b). While superantigen-mediated T cell activation can lead to systemic inflammation as observed in toxic shock syndrome (Low, 2013), the role of T cells in disease pathogenesis of acute MIS-C remains unresolved. Additionally, while SARS-CoV-2–specific T cells can be detected in the children with MIS-C (Conway et al., 2022; Hsieh et al., 2022; Lam et al., 2022), the impact of MIS-C on the generation and functionality of SARS-CoV-2–specific memory T cells compared to children with more typical COVID-19 symptomology remain unclear.

Here, through longitudinal profiling of patients during acute disease and through recovery (up to 19 mo after infection) over the course of the pandemic, we reveal that SARS-CoV-2 infected children with MIS-C exhibit distinct immune activation and memory responses. In the acute phase, children with MIS-C had significantly elevated serum levels of pro-inflammatory (type I) cytokines, while children with acute COVID-19 (COVID) had elevated levels of type II cytokines. T cells in acute MIS-C expressed phenotypic and transcriptional signatures of activated and tissue resident T cells, the latter of which correlated with indicators of cardiac dysfunction. By contrast, T cells in acute COVID exhibited follicular helper T cell (T_{FH}) profiles associated with antibody formation. Long-term follow-up revealed resolution of T cell aberrations in MIS-C–recovered children and higher levels of SARS-CoV-2–specific T cell memory compared to children who recovered from COVID, along with neutralizing antibody activity against multiple viral strains. Our results indicate that activated T cells bearing tissue signatures may contribute to the systemic inflammation and tissue damage that are hallmarks of acute MIS-C but in turn also enable generation of functional protective immune memory.

Results

Clinical cohorts of MIS-C and COVID-19 during acute disease and recovery

In order to investigate the immunological basis of MIS-C relative to other manifestations of SARS-CoV-2 infection in children, we analyzed pediatric subjects over the course of the pandemic for a total of 89 infected and 21 control (uninfected) children comprising three cohorts: (1) children diagnosed with MIS-C (MIS-C); (2) children infected with SARS-CoV-2 who never developed MIS-C (COVID); (3) seronegative children who had no evidence of ongoing or previous SARS-CoV-2 infection or vaccination (see Table 1 for demographics of each cohort and Fig. 1 for a temporal schematic of enrollment over the pandemic). Peripheral blood samples were obtained during the acute phase of disease from children hospitalized for MIS-C or COVID-19. Blood samples were obtained following recovery from MIS-C (MIS-C-R) or COVID-19 (COVID-R) during outpatient visits at timepoints 0.5–19 mo after infection (Table 1). The timing of enrollment for the MIS-C and COVID cohorts is skewed (Fig. 1 and Table 1), attributed to the increased incidence of hospitalized pediatric COVID-19 associated with later variants of SARS-CoV-2 (Martin et al., 2022; Wang et al., 2022). The MIS-C and COVID cohorts were predominantly male and were racially and ethnically diverse (Table 1). Age ranges were mostly consistent across groups, though hospitalized children with acute COVID were younger on average (Table 1).

MIS-C can be classified as severe, moderate, and mild based on clinical severity, ranging from life-threating shock to symptoms that do not require intensive care (Jonat et al., 2021; Sharma et al., 2021). In the MIS-C cohort, clinical severity (see Materials and methods) was evenly distributed among mild and moderate/severe forms, with overall rates of respiratory failure lower in the MIS-C cohort compared to children with acute COVID (Table 2). The MIS-C cohort had a 100% survival rate, while one child out of 16 children with acute COVID died. The majority of the MIS-C subjects received steroid and IVIG treatment during their hospitalization (Table 2). With these cohorts, we sought to define the immunological aberrations in acute MIS-C relative to acute COVID, and determine whether these dysfunctions were resolved during recovery by comparing MIS-C children at extended timepoints after infection to children who recovered from COVID-19 without developing MIS-C. In addition, using samples obtained longitudinally during follow-up visits, we were able to compare the generation and maintenance of SARS-CoV-2–specific humoral and cellular immune memory in these different pediatric cohorts.

Children with MIS-C exhibit distinct cytokine profiles compared to COVID-19

A hallmark of MIS-C and severe COVID-19 (as assessed in adults) is the presence of elevated levels of multiple pro-inflammatory serum cytokines (Consiglio et al., 2020; Diorio et al., 2020; Hadjadj et al., 2020; Lucas et al., 2020; Szabo et al., 2021). The increased incidence of severe pediatric disease seen during the Delta and Omicron waves of SARS-CoV-2 infection enabled us to investigate the inflammatory profile in acute pediatric COVID compared to MIS-C. We compared the serum immune mediator profiles as measured by multiplex analysis from all cohorts (Fig. 2). While recovered cohorts exhibited cytokine profiles similar to seronegative controls, acute disease cohorts exhibited distinct cytokine profiles (Fig. 2 A).

In the acute phase, children with MIS-C and COVID exhibited elevated levels of certain serum cytokines but distinct profiles were observed for each cohorts. Sera from children with MIS-C exhibited upregulation of cytokines associated with type 1 inflammation and antiviral immune responses relative to sera from acute COVID (Fig. 2 B). These MIS-C–specific elevations included TNF-α and CXCL9 (associated with extravasation of lymphocytes to the site of infection), IL-27 (which promotes

Table 1. **Demographics of pediatric cohorts**

	MIS-C[a]		COVID-19		
	Acute	**Recovered**	**Acute**	**Recovered**	**Seronegative**
Subjects (*n*)	22	26	16	36	21
Sex, male, *n* (%)	16 (73)	16 (62)	12 (75)	20 (56)	8 (38)
Age, yr, median (range)	11.2 (4.3–17.2)	9.7 (1.2–16.1)	3.5 (0.07–15)	8.5 (0.42–16)	8.00 (0.75–15)
Months after infection, median (range)	1 (0.5–1)[b]	8 (1.1–19)	0.15 (0.03–0.47)	6.5 (0.5–10)	n/a
Race or ethnicity, *n* (%)					
African American	6 (27)	6 (23)	0 (0)	6 (19)	1 (5)
Hispanic	7 (32)	13 (50)	9 (56)	19 (61)	11 (52)
White	5 (23)	3 (12)	5 (31)	3 (10)	6 (29)
Other	1 (5)	1 (4)	0 (0)	1 (3)	1 (5)
Unknown	3 (14)	3 (12)	2 (13)	2 (7)	2 (9)
Comorbidities, *n* (%)					
Asthma	3 (14)	2 (8)	2 (13)	10 (28)	1 (5)
Cardiac	1 (5)	0	2 (13)	6 (17)	3 (14)
Gastrointestinal	0	0	3 (19)	1 (3)	1 (5)
Endocrine/metabolic	1 (5)	0	1 (6)	2 (6)	2 (10)
Obesity	1 (5)	0	3 (19)	1 (3)	3 (14)
Hematologic	1 (5)	0	1 (6)	1 (3)	1 (5)
Neurological/neuromuscular	0	0	6 (38)	4 (11)	4 (19)
Chronic respiratory	0	0	1 (6)	1 (3)	0 (0)
Other	2 (9)	1 (4)	3 (19)	8 (22)	4 (19)
Variant					
Original	16 (73)	21 (81)	2 (13)	20 (55)	n/a
Alpha	4 (18)	4 (15)	1 (6)	6 (17)	n/a
Delta	0	0	4 (25)	0	n/a
Omicron	2 (9)	1 (4)	9 (56)	5 (14)	n/a
Unknown	0	0	0	5 (14)	n/a

[a]MIS-C cohort comprises 37 unique patients of whom 11 subjects were included in both acute and recovery phases.
[b]Timing of acute infection was unknown or unreported in 13 of 22 acute MIS-C subjects and was presumed to be 1 mo prior to acute presentation, consistent with Feldstein et al. (2020).

differentiation of T helper 1 [T_H1] lineage CD4$^+$ T cells, cytotoxic CD8$^+$ T cells and natural killer [NK] cells), IL-10 (a regulatory cytokine produced by CD8$^+$ T cells in response to respiratory infection; Newton et al., 2016; Sun et al., 2009), and MCP2, a monocyte chemoattractant. By contrast, cytokines elevated in sera from acute COVID subjects included increased levels of CCL15, eotaxin, M-CSF, and IL-13—all of which are associated with type 2 immune responses through their role in eosinophil recruitment, mucus production, M2 macrophage polarization, and T helper 2 (T_H2) responses (Fig. 2 C; Bonecchi et al., 2000; Pope et al., 2001). Both acute MIS-C and acute COVID groups also exhibited elevated expression of IL-15 and IL-6 and downregulation of certain chemokines such as neutrophil attractant CXCL5 compared to recovery and seronegative cohorts (Fig. 2 D). These results show the distinct immunological milieu of acute MIS-C as a systemic inflammatory disease compared to acute COVID, and these profiles are transient features of both disease types.

Altered composition of peripheral blood lymphocytes in children with acute MIS-C

The elevation of cytokines and chemokines that exert direct effects on lymphocytes in acute MIS-C and COVID prompted investigation of lymphocytes across cohorts by flow cytometry (Fig. 3; see gating strategy in Fig. S1 A). Acute MIS-C and acute COVID presented with a decreased frequency of T cells concomitant with an increased frequency of B cells and no significant change in NK/innate lymphoid cells compared to recovered cohorts (Fig. 3 A). These results indicate that changes to the T:B cell ratio previously reported during acute MIS-C (Lee et al., 2020; Vella et al., 2021) are general features of active disease from SARS-CoV-2 infection.

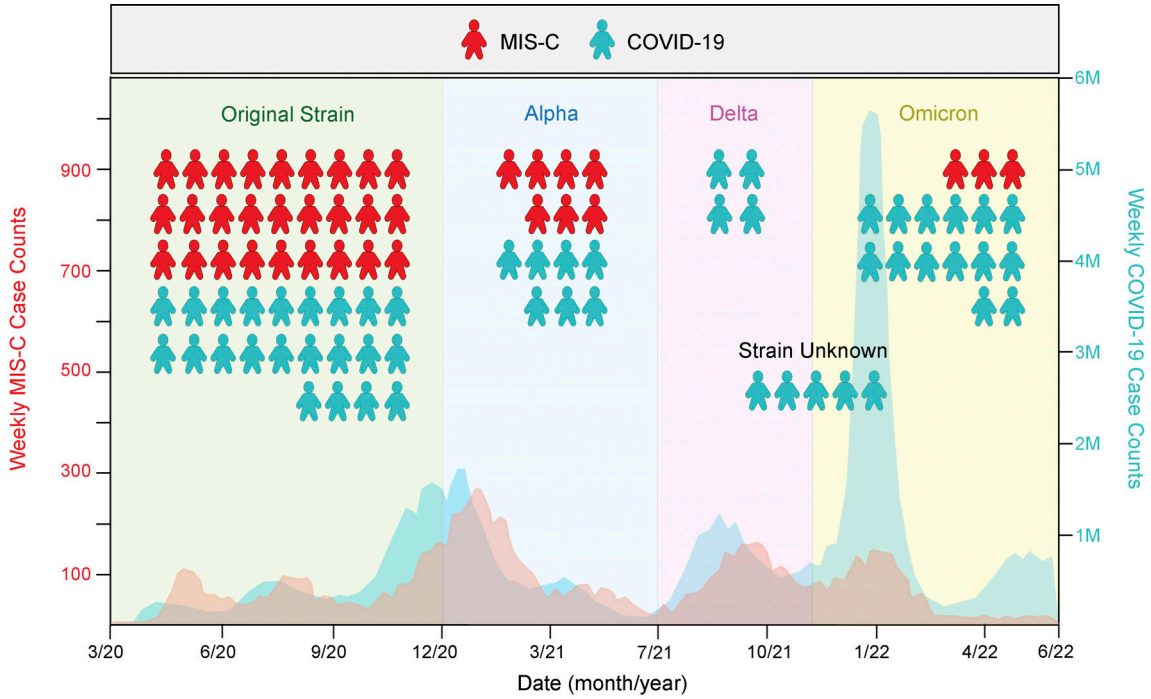

Figure 1. **Enrollment schematic for each subject over the course of the SARS-CoV-2 pandemic.** Visual representation of each subject (MIS-C, *n* = 37; COVID-19, *n* = 52) recruited for this study superimposed on the wave during which they were infected. The number of weekly MIS-C cases is depicted in red (left y axis), and number of weekly COVID-19 cases depicted in blue (right y axis). Case data were sourced from the Center for Disease Control (https://covid.cdc.gov/covid-data-tracker/#mis-national-surveillance).

Table 2. **Clinical characteristics of patients in MIS-C study**

	Acute MIS-C[a]	Acute COVID-19
Severity, *n* (%)		
MIS-C mild	17 (46%)	n/a
MIS-C moderate	10 (27%)	n/a
MIS-C severe	10 (27%)	n/a
Respiratory failure	9 (24%)	10 (63%)
ARDS	4 (11%)	5 (31%)
ECMO	0 (0%)	2 (13%)
Survival	37 (100%)	15 (94%)
Treatment, *n* (%)		
Steroids	37 (100%)	11 (69%)
IVIG	36 (97%)	0 (0%)
Remdesivir	1 (3%)	9 (56%)
Immune modulator[b]	8 (21%)	0 (0%)

ARDS, acute respiratory distress syndrome; ECMO, extracorporeal membrane oxygenation.
[a]Includes clinical data for acute presentation even if no biologic sample obtained.
[b]All patients received Anakinra.

There were comparable $CD4^+$ and $CD8^+$ T cell frequencies across acute and recovered cohorts, suggesting that the decreased frequency of peripheral blood T cells in acute MIS-C was not due to biased decreases in either $CD4^+$or $CD8^+$ T cell populations (Fig. 3 B). In analyzing T cell subset proportions, MIS-C-R children had a greater frequency of double-negative and γδ T cells compared to the other cohorts (Fig. 3 B). We further investigated whether there were specific changes in $CD4^+$ and $CD8^+$ T cell memory subsets (Fig. 3 C). No significant differences were identified, suggesting a pan-decrease in circulating T cell subsets during acute MIS-C and acute COVID. These results indicate transient yet dynamic changes in peripheral T cell subsets during acute disease, which are largely resolved during recovery.

Expression of tissue resident markers by circulating T cells is a distinct feature of acute MIS-C

We performed an in-depth analysis of T cell phenotypes in the different disease cohorts during acute disease and recovery by high dimensional flow cytometry. Our analysis included markers for activation (CD38, HLA-DR, CD69), tissue residence (TRM; CD103, CD49a; Kumar et al., 2017; Szabo et al., 2019a) inhibition (PD-1; Wherry, 2011), and T_{FH} cells (CXCR5; Crotty, 2011; Fig. 4 and Fig. S2). These markers were mostly expressed by memory rather than naive T cells as shown in representative flow cytometry plots (Fig. 4 A and Fig. S2 A). Memory-phenotype T cells in both acute MIS-C and COVID subjects showed elevated levels of the activation marker HLA-DR (Fig. 4 B). However, each cohort exhibited differential expression of additional phenotypic

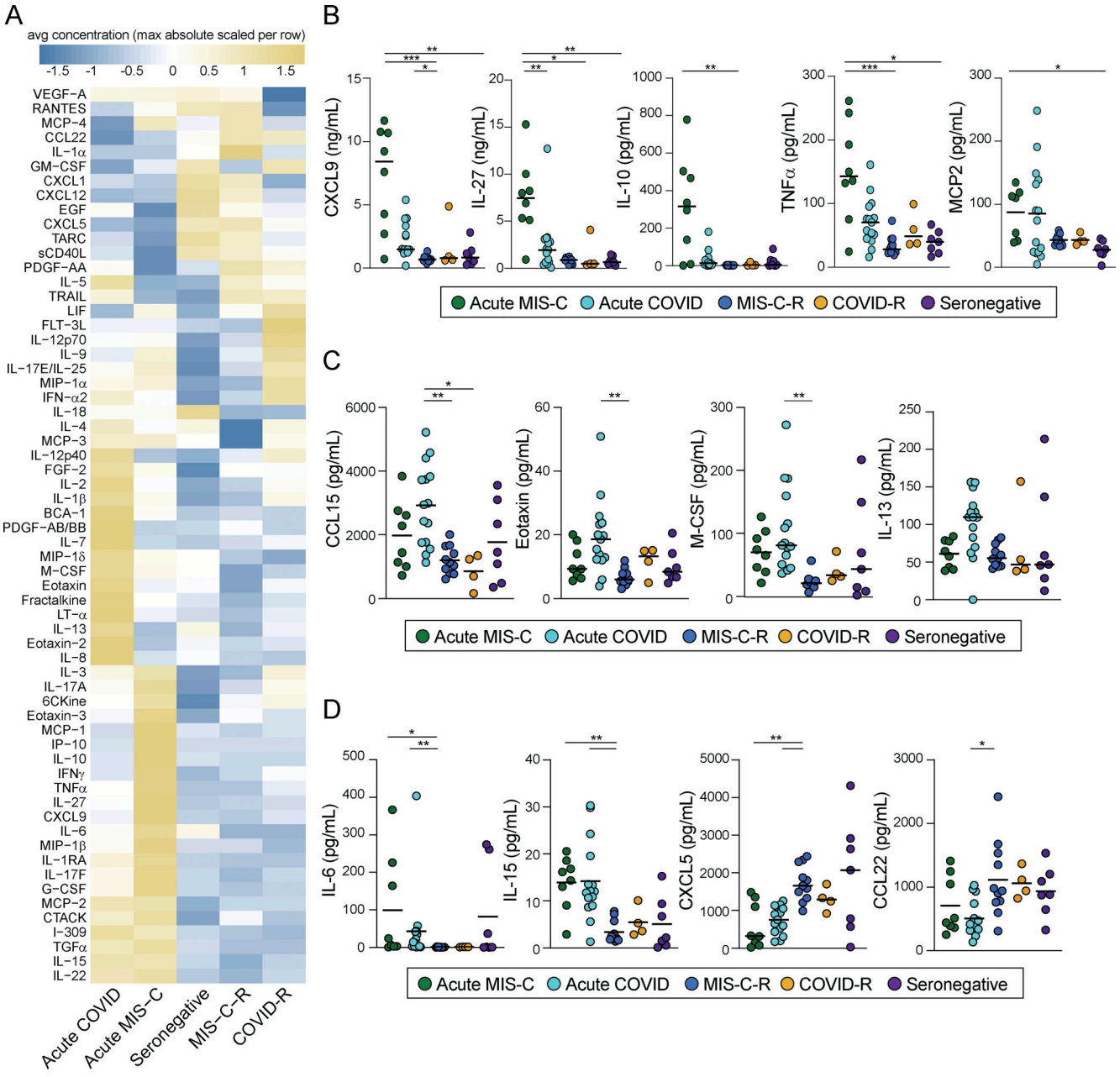

Figure 2. **Distinct immune mediator profiles in acute MIS-C and COVID-19 are resolved in recovery. (A)** Profiles of immune mediators present in plasma shown as a heatmap and stratified by cohort; acute MIS-C (n = 8), acute COVID (n = 15), MIS-C-R (n = 11), COVID-R (n = 4), seronegative (n = 7). Color intensity of each cell represents analyte concentration (maximum absolute scaled per row) within each cohort. Unsupervised clustering of cytokine expression was done using complete method (distance metric: Euclidean). **(B)** Analytes found to be elevated during acute MIS-C. **(C)** Analytes increased during acute COVID. **(D)** Analytes found to be elevated or reduced in both acute MIS-C and acute COVID. **(B–D)** Concentration of indicated immune mediators present in plasma. Statistical analyses were performed using Kruskal–Wallis test with Dunn's correction. Line depicts median. *, P < 0.05; **, P < 0.01; ***, P < 0.00.

markers. Memory CD4⁺T cells from acute MIS-C expressed significantly higher frequencies of canonical TRM markers CD49a and CD103 (Kumar et al., 2017) compared to T cells in acute COVID, recovery, and control groups (Fig. 4 B). Similarly, memory CD8⁺T cells from acute MIS-C exhibited upregulation of TRM markers CD49a and CD69 relative to the other groups (Fig. 4 B). By contrast, T cells from acute COVID had elevated expression of both PD-1 and CXCR5 compared to acute MIS-C and recovered groups; co-expression of these markers identified elevated frequencies of T_{FH} cells in acute COVID relative to MIS-C (Fig. 4 B). These results show aberrant T cell responses in acute MIS-C bearing signatures of tissue residency, while T cells in acute COVID-19 show features of normal T_{FH} differentiation, important for promoting antibody responses to primary infection.

We further examined expression differences in TRM and activation markers in MIS-C subjects pairing acute and recovery samples (Fig. 4 C). Increased expression of CD69,

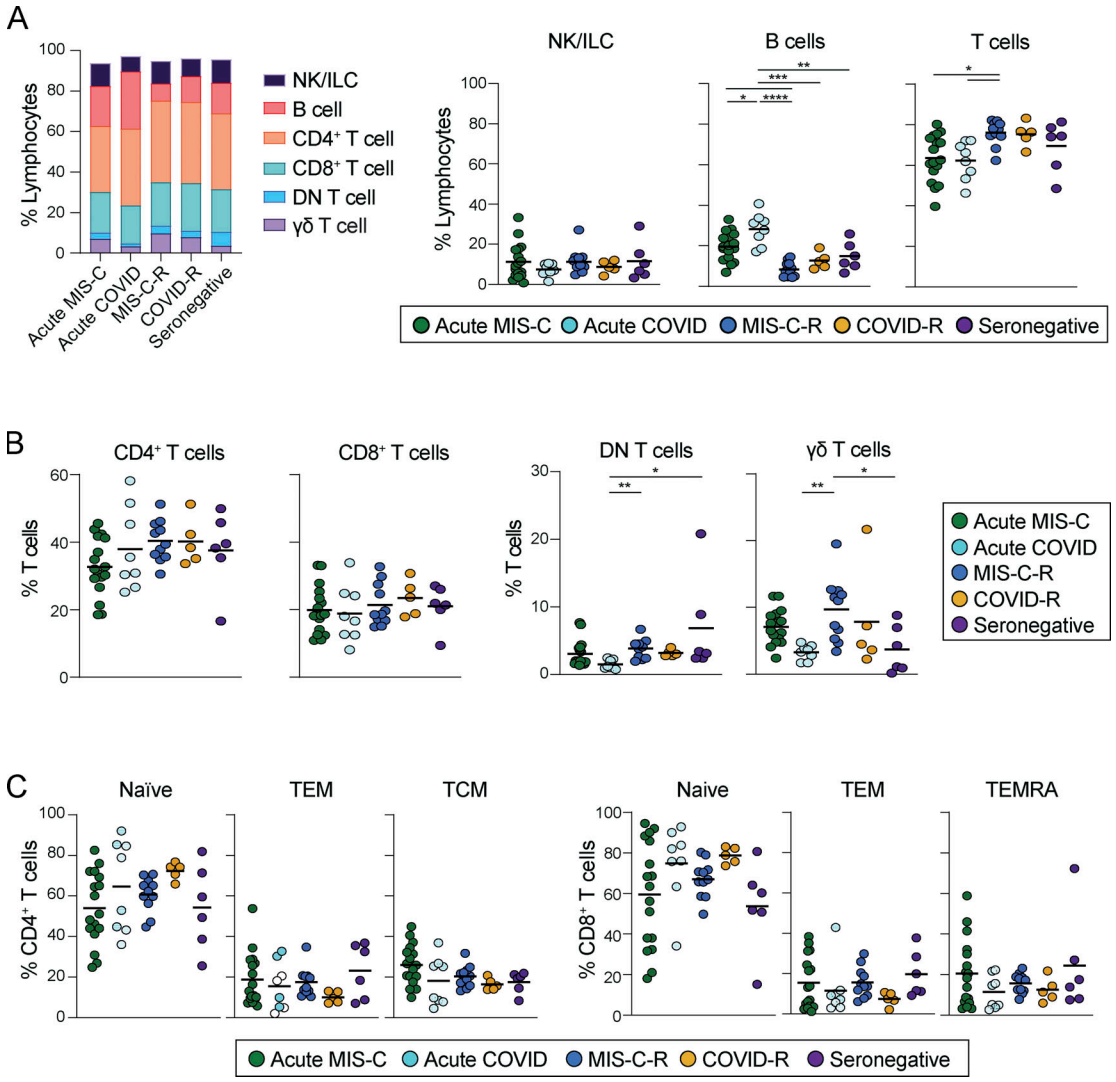

Figure 3. **Similar alterations in immune cell frequencies during acute MIS-C and COVID are resolved during recovery.** Lymphocyte subset frequencies were assessed from peripheral blood samples of acute MIS-C (n = 17), acute COVID (n = 8), MIS-C-R (n = 11), COVID-R (n = 5), and seronegative (n = 6). **(A)** Bar graph (left) depicting distributions of major lymphocyte populations with breakdown of lymphocyte subsets (right) organized by cohort. **(B)** Frequencies of CD3⁺ T cell subsets by cohort. **(C)** Frequencies of CD4⁺ (left) and CD8⁺ (right) T cell memory subsets based on expression of CD45RA and CCR7 delineating naive (CD45RA⁺CCR7⁺), central memory (TCM; CD45RA⁻CCR7⁺), terminal effector (TEMRA; CD45RA⁺CCR7⁻), and effector-memory (TEM; CD45RA⁻CCR7⁻) cells by cohort. Lines depict mean. Statistical analysis was performed using one-way ANOVA with Tukey's correction. *, P < 0.05; **, P < 0.01; ***, P < 0.001; ****, P < 0.0001. NK/ILC, NK cell/innate lymphoid cell; DN, double-negative T cell.

CD103, and PD-1 during the acute phase of disease did not persist into recovery (Fig. 4 C and Fig. S2 B). Moreover, in acute MIS-C, there was co-expression of activation and TRM markers (CD38, HLA-DR, CD103, PD-1) with CD49a, an integrin which functions in TRM tissue surveillance following viral infections (Reilly et al., 2020; Fig. 4 D). Together, these findings suggest that activated, tissue-derived T cells are present in peripheral blood during acute MIS-C but do not persist upon restoration of tissue homeostasis in recovered individuals.

Expression of TRM phenotypes correlate with clinical manifestations of MIS-C

We investigated whether aberrant T cell phenotypes observed in acute MIS-C correlated with clinical measures of disease severity. Severe cardiac inflammation and dysfunction were among the most prominent and concerning clinical presentations of acute MIS-C (Cheung et al., 2020). In order to define the scope of cardiac disease within this MIS-C cohort, we analyzed blood and echocardiographic markers of cardiac function and ischemia obtained during acute MIS-C and follow-up appointments (2–19 mo after infection; Fig. 5 A). Upon admission, the majority (62%) of subjects presented with elevated levels of troponin T (median, 26 ng/liter; range, <6–2,445; reference, <22 ng/liter) indicating ischemia, and increased N-terminal pro-brain-type natriuretic peptide (NT-proBNP; median, 5,741 pg/ml; range, 452.8–>70,000; reference, <207 pg/ml), an indicator of heart failure, suggesting significant cardiac dysfunction based on blood indicators (Fig. 5 A). To directly assess heart function, we used ejection fraction (EF) measured on echocardiogram, which revealed near normal systolic

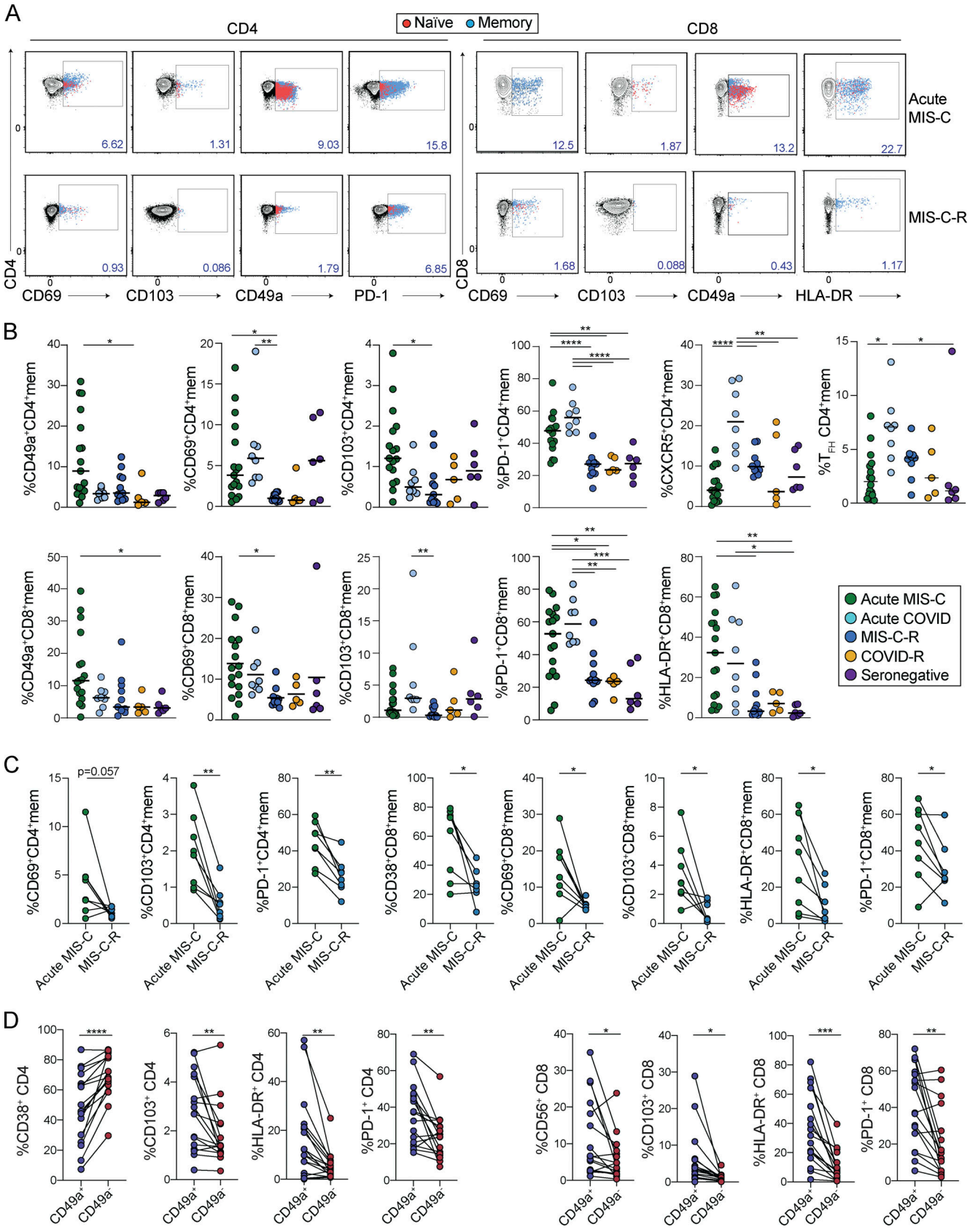

Figure 4. **Distinct T cell phenotypes in acute disease groups suggest aberrant responses in MIS-C. (A)** Representative flow cytometry plots of CD4+ (left) and CD8+ (right) T cells by expression of markers of activation (CD69, HLA-DR, PD-1) and tissue residency (CD49a, CD103) during acute MIS-C (top) and MISC-R (bottom). **(B)** Frequency of expression of selected markers on memory CD4+ (top) and CD8+ (bottom) T cells organized by cohort; acute MIS-C (*n* = 17), acute

COVID (n = 8), MIS-C-R (n = 11), COVID-R (n = 5), and seronegative (n = 6) controls. T_{FH} cells defined by co-expression of PD-1 and CXCR5. Lines represent median for each cohort. Statistical analyses were performed using ordinary one-way ANOVA with Tukey's correction or Kruskal–Wallis testing with Dunn's correction. **(C)** Paired analysis of marker expression on memory CD4⁺ (left) and CD8⁺ (right) T cells during acute MIS-C and following recovery. Statistical analyses were performed using paired t test. **(D)**. Paired analysis of marker expression on CD49a⁺ and CD49a⁻ subsets in CD4⁺ (left) and CD8⁺ (right) T cells in acute MIS-C children. Statistical analyses were performed using paired t test. *, P < 0.05; **, P < 0.01; ***, P < 0.001; ****, P < 0.0001. Mem, memory.

function (55–70% EF) in approximately half (51%) of acute MIS-C subjects while others had severely decreased EF (<40% EF; Fig. 5 A). Paired analysis of these acute manifestations to short-term (2–6 mo) and longer-term (6–19 mo) follow-up data showed normalization of blood and echocardiographic findings for all subjects, similar to recent clinical studies of MIS-C (Farooqi et al., 2021; Matsubara et al., 2022).

We investigated whether aberrant expression of T cell activation or tissue residency markers during acute MIS-C (Fig. 4) correlated with indicators of cardiac dysfunction, specifically troponin and EF that had varied widely across the cohort. Interestingly, there were significant correlations in the expression of TRM markers with increased troponin or reduced EF, as markers of cardiac dysfunction and worsening disease (Fig. 5 B). Specifically, the proportion of CD103-expressing CD4⁺T cells was higher with increased troponin, and the proportion of CD49a-expressing CD8⁺T cells was inversely correlated with EF, while none of the markers for activation (CD38, HLA-DR) demonstrated a statistically significant correlation to increased disease severity (Fig. 5 B). These results indicate that certain types of TRM in circulation are associated with increased disease severity and could serve as potential biomarkers for clinical outcomes during acute disease.

Transcriptional signatures and TCR clonal expansions in acute MIS-C T cells are resolved in recovery

The correlation of TRM phenotypes with disease severity in MIS-C patients and the resolution of these aberrations in recovery suggested a role for T cells in the disease process. We therefore performed in-depth molecular profiling of T cells in acute MIS-C and MIS-C-R by analysis of gene expression and clonal analysis of TCR gene sequences (Fig. 6). To investigate gene expression changes in CD4⁺ and CD8⁺ T cells isolated from peripheral blood of children during acute MIS-C and recovery, we used whole transcriptome profiling by RNA sequencing (RNAseq; Fig. 6, A and B). Differential gene expression (DEG) analysis of acute versus recovered subjects revealed a limited number of significantly differentially expressed genes, many of which were associated with T cell activation, proliferation, and tissue residency (Fig. 6 A, Table S1, and Table S2). Consistent

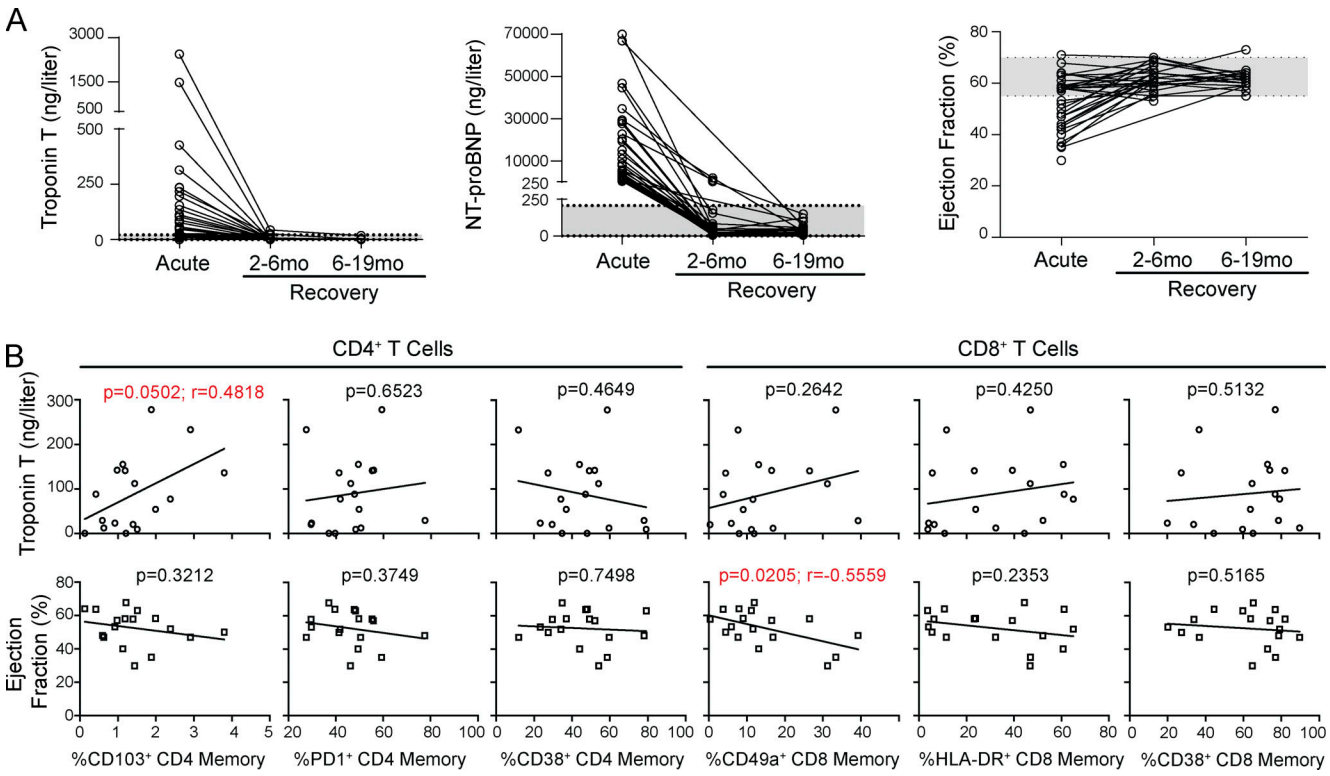

Figure 5. **Aberrant expression of TRM markers correlate with cardiac disease severity during acute MIS-C. (A)** Paired serological and echocardiographic cardiac clinical data from MIS-C subjects at acute (n = 35–37) and recovery (2–6 mo; n = 32 and 6–19 mo; n = 17–18 after infection) timepoints. Dotted lines with gray shading represent normal ranges for each parameter. **(B)** Correlation analysis (n = 17) of T cell subsets (x axis) to cardiac testing (y axis); troponin T (top) or EF (bottom). Statistical testing was done with Pearson correlation.

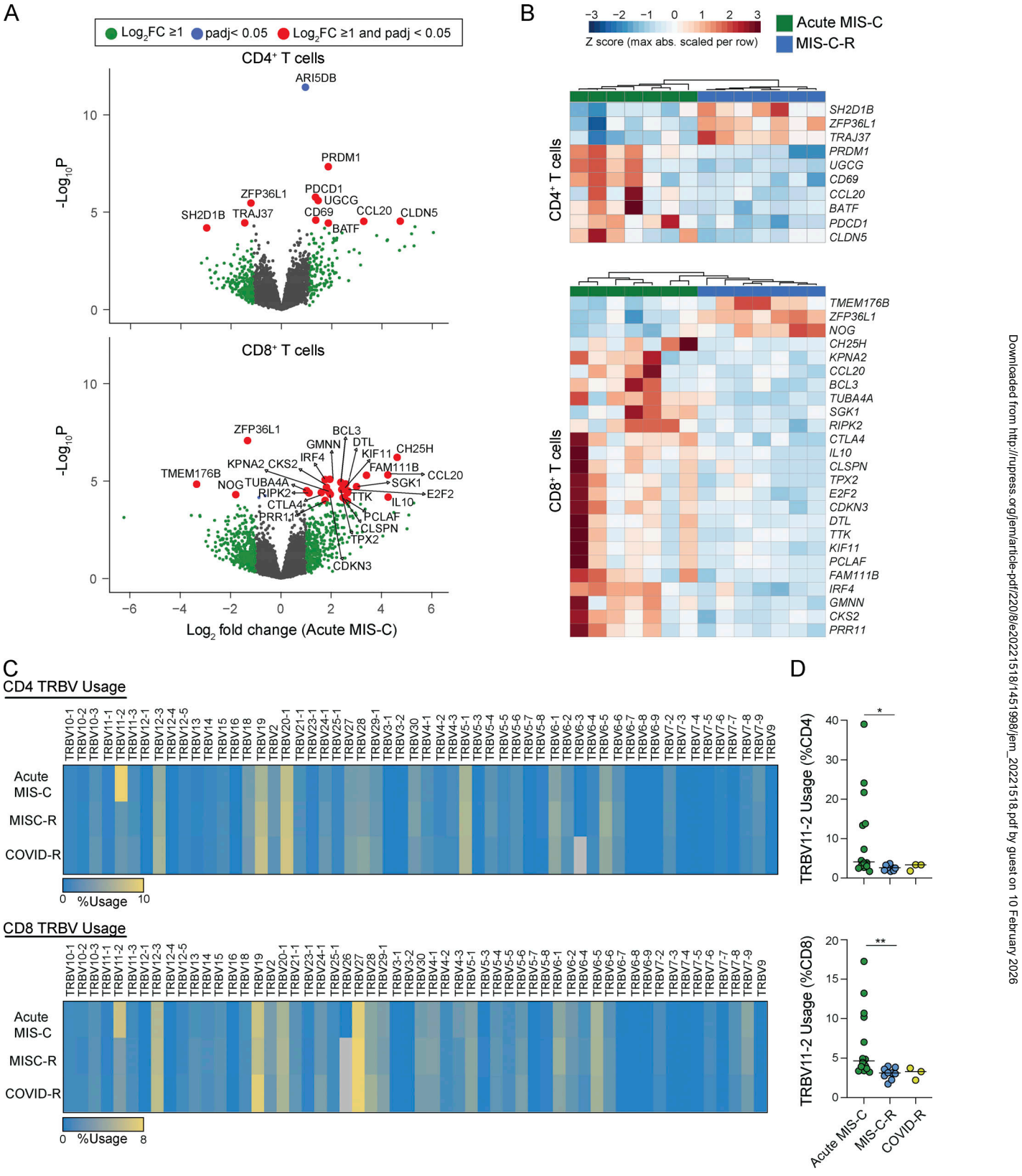

Figure 6. **Distinct transcriptional signatures and TCR clonal expansions of MIS-C resolve following recovery. (A)** Volcano plots of differentially expressed genes in CD4⁺ (top) and CD8⁺ (bottom) T cells between acute MIS-C (n = 7) and MIS-C-R 6–12 mo after infection (n = 7) subjects. Log fold change describes upregulation or downregulation of a given gene in acute MIS-C in comparison to MIS-C-R. **(B)** Heatmaps of normalized mean counts of significantly differentially expressed genes in CD4⁺ (top) and CD8⁺ (bottom) T cells between acute MIS-C (green) and MIS-C-R (blue) cohorts. Subjects in heatmaps were clustered by complete cluster function (see Materials and methods). Genes were significantly different if they had a $\log_2$FC ≥1 and an adjusted P value <0.05.

(C) Heatmap depicting TCR Vβ-chain usage in CD4⁺ (top) and CD8⁺ (bottom) T cells isolated from peripheral blood of acute MIS-C children and following recovery compared to COVID-R. Color intensity represents frequency of chain usage as a percentage of the total repertoire. **(D)**. Frequency of *TRBV11-2* usage in CD4⁺ (top) and CD8⁺ (bottom) peripheral blood repertoires in acute MIS-C children, MISC-R, and COVID-R subjects. Lines depict median for each cohort. Statistical analyses were performed using Kruskal–Wallis test with Dunn's correction. *, P < 0.05; **, P < 0.01.

with the flow cytometry results, CD4⁺ T cells in acute MIS-C showed an upregulation of *PDCD1* (encoding PD-1) and genes related to tissue residency including *CD69*, *PRDM1* (encoding for a transcription factor for TRM development; Mackay et al., 2016), *BATF*, and *CCL20* (Chen et al., 2021; Kumar et al., 2017; Szabo et al., 2019b).

CD8⁺T cells in acute versus recovery showed upregulation of genes associated with activation, tissue residency, and migration, including *TUBA4A*, *IRF4*, and *CCL20* (Kumar et al., 2017; Szabo et al., 2019a), along with *CTLA4*, an early activation marker and *IL10*, a key regulatory cytokine. CD8⁺T cells in acute MIS-C also showed upregulated expression of *SGK1* (encoding serum- and glucocorticoid-regulated kinase 1) expressed by T cells mediating end organ damage through an angiotensin II–directed pathway (Norlander et al., 2017), also activated in severe COVID-19 (Miesbach, 2020). Together, this analysis reveals gene expression profiles in circulating T cells of acute MIS-C that exhibit features of activation, tissue residency, and dysregulation, which do not persist during recovery, consistent with our flow cytometry analysis and further supporting a pathogenic role of T cells during acute MIS-C.

We also interrogated the clonal distribution of T cells in acute MIS-C compared to MIS-C-R and COVID-R cohorts. We sequenced the *TRBV* gene within the Vβ and CDR3 region as described (Miron et al., 2021) of sorted peripheral blood CD4⁺ and CD8⁺ T cells from the different cohorts (Fig. 6 C and Table S3). Heat maps show biased expression of *TRBV11-2* in CD4⁺ and CD8⁺T cells (Fig. 6 C) from acute MIS-C compared to the other groups consistent with findings of expanded *TRVB11-2* in other cohorts (Cheng et al., 2020; Noval Rivas et al., 2021; Porritt et al., 2021a, 2021b). Comparison of the frequency of CD4⁺ or CD8⁺T cells expressing *TRBV11-2* demonstrated a marked increase during acute MIS-C that was not observed in MIS-C-R or COVID-R subjects (Fig. 6 D). These results confirm previous reports of biased expansion of *TRBV11-2*–expressing T cells in acute MIS-C and reveal that this expansion is transient, with the frequency of *TRBV11-2* in MIS-C-R children similar to COVID-R children.

Children with MIS-C generate functional SARS-CoV-2–specific immune memory with enhanced anti-viral cellular responses

We asked whether the SARS-CoV-2–specific memory response differed in MIS-C-R compared to COVID-R children (Fig. 7), given their distinct profiles in acute disease. Virus-specific T cells were detected using the well validated activation-induced marker (AIM) assay in which peripheral blood mononuclear cells (PBMCs) are cultured with peptide megapools (MPs) containing SARS-CoV-2 T cell epitopes, and virus reactivity is measured by upregulation of markers associated with antigen-driven activation (Grifoni et al., 2020). The extent of virus reactivity was defined by upregulation of two or three activation markers (see Materials and methods; Fig. 7 A).

For CD4⁺ T cells, MIS-C-R children exhibited responses to SARS-CoV-2–specific peptides including the Spike (S) protein and other viral proteins at significantly higher levels compared to COVID-R and seronegative children, which exhibited comparably low virus-reactivity (Fig. 7 B). For CD8⁺T cells, children in both MIS-C-R and COVID-R groups had variable but low frequencies of virus-reactive T cells, though there were no significant differences between groups (Fig. 7 B). In order to assess functional responses distinct from activation-marker induction, we assessed the cytokine profile of virus-specific T cells (Fig. 7 C). Notably, CD4⁺T cells from MIS-C-R subjects produced higher levels of IL-2, while virus-reactive CD8⁺T cells in MIS-C-R subjects produced significantly higher levels of TNF-α and IFN-γ compared to COVID-R subjects (Fig. 7 C). These findings reveal that virus-specific memory CD4⁺ and CD8⁺T cells are generated following infection in children, but that subjects who recovered from MIS-C exhibited a more robust functional memory response compared to infected children who did not develop MIS-C.

To assess whether the different memory T cell responses in MISC-R compared to COVID-R were due to differences in age, viral variant, and time from infection, we performed a multivariate analysis. Our results indicate that clinical cohort is the major determinant of SARS-CoV-2 T cell responses (Table S4). Together, these results show that T cell memory generated in MIS-C is quantitatively and qualitatively distinct with a higher frequency and T_H1-like functional profile compared to T cell memory generated in COVID-R subjects, which is lower in magnitude and functionality.

Infected pediatric cohorts maintain similar SARS-CoV-2–specific antibody profiles and dynamics

Finally, we compared antibody response profiles in children with MIS-C to children with COVID-19 in the acute phase and following recovery; in addition, serum sampling at multiple recovery timepoints enabled us to follow the dynamics of this response. All infected cohorts were able to generate IgG and IgA antibodies specific for the SARS-CoV-2 S protein, IgG antibodies against the receptor-binding domain (RBD) of the S protein, and IgG antibodies specific for nucleocapsid (N) protein at levels significantly higher than seronegative controls (Fig. 8 A). During the acute phase, children with MIS-C had significantly higher magnitudes of IgG and IgA anti-S, IgG anti-RBD, and IgG anti-N antibodies compared to children with acute COVID, who exhibited greater variability in antibody levels (Fig. 8 A). When comparing acute and recovered groups, there was an increase in anti-S and anti-N antibodies in recovered compared to acute disease for the COVID-19 cohort, while the MIS-C cohort exhibited comparable anti-S and anti-RBD antibody levels, except for a reduction in anti-S IgA and anti-N antibodies in recovery versus acute timepoints (Fig. 8 A). Across disease severity,

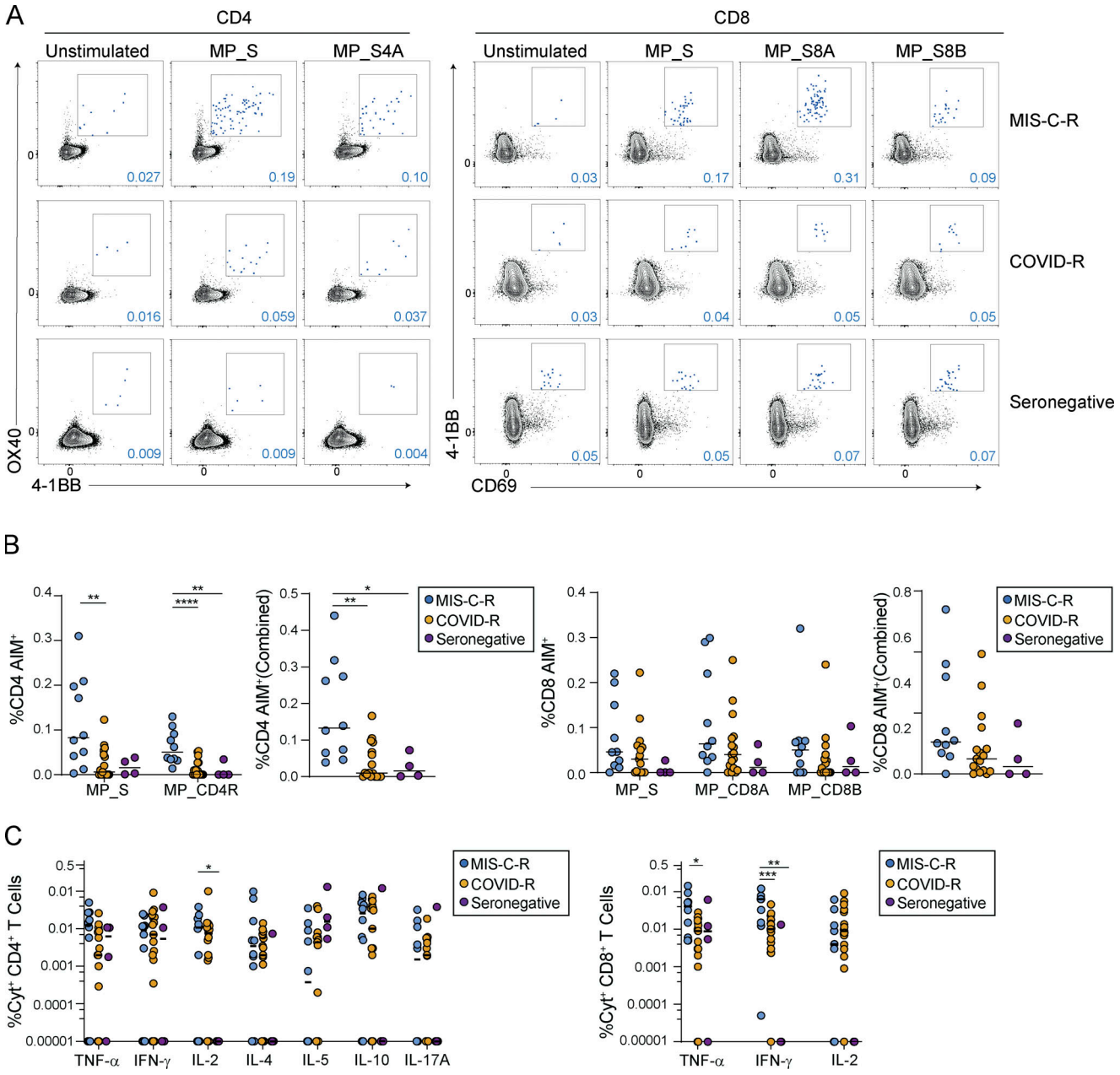

Figure 7. **Enhanced frequency and functionality of memory T cells in children who recovered from MIS-C versus COVID-19. (A)** Representative flow cytometry data identifying SARS-CoV-2–specific CD4+ (left) and CD8+ (right) T cells using the AIM assay (see Materials and methods) based on the induction of OX40, 4-1BB, and CD40L. Data organized by cohort (row) and peptide pool (columns; CD4; MP_S, MP_CD4R or CD8; MP_S, MP_CD8A, MP_CD8B—see Materials and methods). **(B)** Frequency of epitope-specific CD4+ (top) and CD8+ (bottom) T cells grouped by clinical cohorts (MISC-R, *n* = 10; COVID-R, *n* = 17; seronegative, *n* = 4) in individual peptide pools and combined reactivity. Lines depict mean for each cohort. Statistical analyses were performed using one-way ANOVA with Tukey's correction or Kruskal–Wallis test with Dunn's correction. **(C)** Frequency of cytokine-positive CD4+ (top) and CD8+ (bottom) T cells following SARS-CoV-2 peptide stimulation from subjects shown in B. Line depicts median. Statistical analyses were performed using Kruskal–Wallis test with Dunn's correction. *, P < 0.05; **, P < 0.01; ***, P < 0.001; ****, P < 0.0001. All samples were between 3–12 mo after infection.

MIS-C children exhibited comparable levels of anti-S, -RBD, and -N antibodies during the acute and recovery phase (Fig. S3 A).

We further assessed the dynamics of SARS-CoV-2–specific antibodies in longitudinal samples for the two cohorts (Fig. 8, B and C). COVID-R subjects exhibited comparable antibody levels of anti-S and anti-RBD IgG antibodies up to 11 mo after infection but a significant decline in anti-N IgG levels (Fig. 8 B). MIS-C subjects also exhibited comparable levels of these antibodies, except for a significant decline in anti-S IgA (Fig. 8, B and C). For the MIS-C children in which multiple longitudinal samples were obtained from the same individual, the magnitude of anti-S, anti-RBD, and anti-N antibody titers was maintained up to 19 mo after infection (Fig. S3 B). In a multivariate model including cohort, age, time from infection, and SARS-CoV-2 variant, the only significant association that emerged was between reduced antibody levels in acute COVID (Table S5). These results indicate

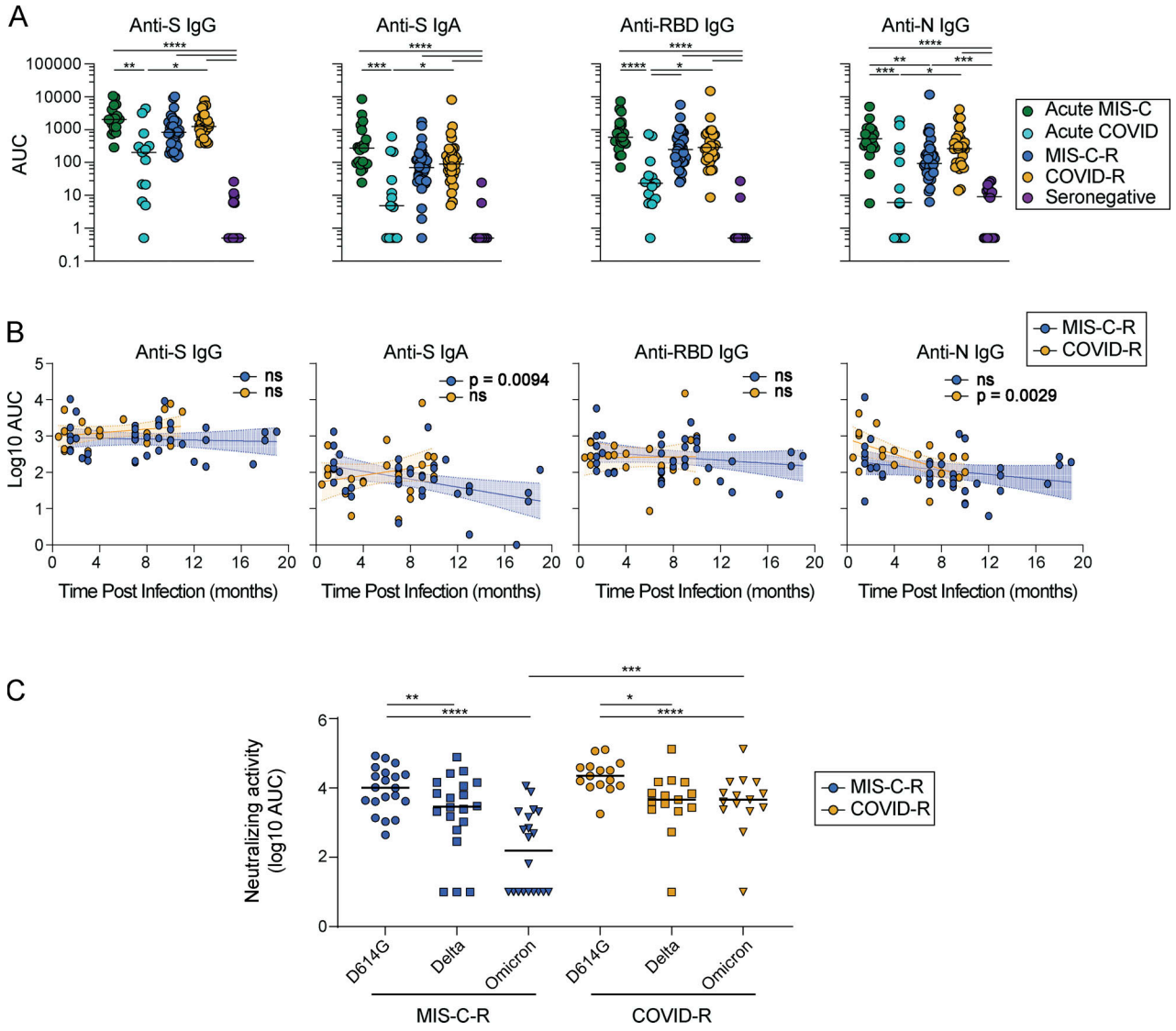

Figure 8. **Longitudinal profiling of antibody responses during acute disease and recovery. (A)** SARS-CoV-2 antibody reactivities in acute MIS-C (n = 18–22), acute COVID-19 (n = 12–13), MIS-C recovered (MIS-C-R; n = 36), COVID recovered (COVID-R; n = 29–31), and seronegative controls (n = 16). Graphs depict IgG and IgA titers by area under curve (AUC) against SARS-CoV-2 Spike (S), RBD, and N proteins, stratified by clinical cohort. Lines depict median. Statistical analyses were performed using Kruskal–Wallis test with Dunn's correction. **(B)** Log-transformed longitudinal analysis of SARS-CoV-2–specific antibodies in MISC-R (n = 36) and COVID-R (n = 24–25) cohorts. Line represents best fit with shading depicting 95% confidence bands. Statistical testing was performed with linear regression. **(C)** Compiled data from pseudotype neutralization assay (see Materials and methods) grouped by cohort (MISC-R, n = 20; and COVID-R, n = 15) and organized by variant vs. log-transformed AUC for neutralizing activity. Statistical testing within cohorts by one-way ANOVA with Tukey's correction and across groups by variant using Mann–Whitney t test. *, P < 0.05; **, P < 0.01; ***, P < 0.001; ****, P < 0.0001.

no bias in antibody levels or persistence in the different clinical cohorts.

We further assessed the protective ability of antibodies to neutralize infection by different viral strains including the ancestral (D614G), Delta variant of 2021–2022, and the more recent Omicron variant using a pseudovirus neutralization assay (Stelitano et al., 2021; Weisberg et al., 2021). Sera from both MIS-C-R and COVID-R subjects exhibited neutralizing activity that was highest against the ancestral strain, lower against the Delta variant, and greatly reduced to the Omicron variant (Fig. 8 C). This hierarchy in neutralization levels to the different strains is consistent with findings in adults (Evans et al., 2022; Schmidt et al., 2022). Antibodies from MIS-C-R subjects demonstrated decreased neutralization activity to Omicron compared to COVID-R subjects, suggesting decreased protection against emerging strains (Fig. 8 C). We applied our multivariate model to determine if additional factors contributed to the observed differences. Similar to the results observed for T cell virus-specific memory (Fig. 7), clinical cohort (namely MIS-C-R) remained the main determinant of reduced neutralization activity to variant strains (D614G and Omicron) when controlling for age, time from infection, and variant (Table S6). Together, these findings establish that humoral immunity is comparably generated in the two disease cohorts and that the major distinguishing immune feature is the T cell response.

Discussion

The immunological mechanisms implicated in MIS-C and their related outcomes in affected children have been difficult to assess. Here, we present longitudinal immune profiling of children who developed SARS-CoV-2–associated MIS-C during acute disease and 1–19 mo following recovery, relative to children with more typical clinical manifestations of SARS-CoV-2 infection over the different waves of the pandemic. We identified a distinct inflammatory mediator profile in acute MIS-C, along with phenotypic, transcriptional, and clonal alterations in T cells during acute disease. In particular, T cells in acute MIS-C upregulated expression of TRM markers, which correlated with clinical measurements of cardiac damage, suggesting tissue infiltration or egress during acute disease. While aberrant T cell phenotypes and inflammation resolved during recovery, children with prior MIS-C generated increased frequencies of functionally robust virus-specific T cells compared to children who recovered from more typical COVID-19 infection. Together our results reveal that the T cell response in acute MIS-C correlated with disease pathology, while also generating robust memory responses important for future immune protection.

Acute MIS-C subjects exhibited unique immune mediator profiles in plasma, with distinctly high levels of CXCL9, IL-27, and TNF-α, consistent with previous analysis of acute MIS-C serum (Consiglio et al., 2020; Gruber et al., 2020; Hoste et al., 2022; Sacco et al., 2022). This type of proinflammatory immune response is associated with extravasation of lymphocytes to the site of infection, consistent with the excessive vasculitis observed in MIS-C. Acute MIS-C sera also had elevated levels of IL-10, a cytokine produced later in infection which can attenuate excessive inflammation (Rojas et al., 2017). By contrast, children with acute COVID exhibited a type 2 immune response characterized by elevated levels of CCL15, eotaxin, IL-13, and M-CSF, consistent with other reports of cytokine profiles in SARS-CoV-2–infected children (Pierce et al., 2020; Ravichandran et al., 2021). Interestingly, a similar cytokine profile is associated with pediatric responses to other respiratory viruses including respiratory syncytial virus and rhinovirus (Becker, 2006; Yuan et al., 2020), suggesting that this profile is a general feature of a protective primary anti-viral response. Together, these results indicate that MIS-C has a distinct and aberrant inflammatory profile associated with disease pathology.

Our examination of adaptive immunity in acute MIS-C relative to other pediatric cohorts implicates a possible role for T cells in immune pathology and tissue damage. Notably, we found that circulating T cells during acute MIS-C exhibit multiple features of tissue-resident T cells, some of which correlate directly with measures of cardiac damage. T cells in acute MIS-C express canonical integrins (CD103, CD49a), the gene *PRDM1*, which encodes the transcription factor Blimp-1, critical for TRM formation (Mackay et al., 2016), and other tissue signature genes (*TUBA4A*, *PDCD1*; Szabo et al., 2019a). This transient expression of TRM signatures by T cells in peripheral blood is rarely observed (Szabo et al., 2019a) and importantly, was not observed in peripheral blood T cells of children with acute COVID (this study), or in adults with severe COVID and acute lung damage (Szabo et al., 2021). Activated T cells were also found in circulation of children with acute COVID but these exhibited phenotypes of T_{FH} cells, involved in a normal primary immune response to respiratory viruses—further evidence that immune responses in MIS-C are aberrant and those in acute COVID are productive.

We propose that TRM phenotype in MIS-C could derive from two possible mechanisms: One possibility is that T cells directly participating in myocarditis and cardiac damage acquire TRM phenotypes and re-emerge in the periphery due to their egress from the inflamed site. This mechanism is supported by correlations we identified between T cells expressing TRM markers and indicators of heart dysfunction, and that the loss of these aberrant T cells in longitudinal follow-up correlated with recovery of cardiovascular health. Another possibility is that TRM cells derive from infection-mediated disruption of the intestinal barrier, which can occur during acute MIS-C (Bajaj et al., 2021; Yonker et al., 2021), thus enabling egress of TRM into circulation. This latter mechanism would therefore implicate an indirect role for T cells in cardiac damage through induction of systemic inflammation.

Further T cell dysregulation in acute MIS-C included the biased expansion of T cells harboring Vβ11-2 TCR chains, consistent with previous findings by other groups (Noval Rivas et al., 2021; Porritt et al., 2021b). This biased expansion resembles superantigen-mediated activation, and it has been proposed that the SARS-CoV-2 S protein can act as a superantigen (Noval Rivas et al., 2022). However, these expansions only occur in a fraction of MIS-C patients, and a previous study did not find a correlation between detectable SARS-CoV-2–reactive T cells and Vβ11-2 expansions (Lam et al., 2022). We propose that this biased expansion could derive from egress of tissue T cells, such as TRM, which can exhibit site-specific expansions (Miron et al., 2021). That the expanded Vβ11-2 T cells do not persist following recovery (at least as measured in blood) suggests these clones either underwent apoptosis and/or were sequestered back in tissues.

Despite the significant T cell alterations during acute MIS-C, recovered children generated functional and more robust SARS-CoV-2–specific T cell memory compared to children who recovered from COVID-19. Encouragingly, these memory lymphocytes were also able to elicit appropriate anti-viral responses upon antigen re-exposure expanding on the results observed by others at shorter timepoints (Conway et al., 2022; Hsieh et al., 2022; Lam et al., 2022; Sacco et al., 2022). We demonstrate that children recovered from MIS-C can maintain SARS-CoV-2–specific antibodies in circulation up to 19 mo after infection at comparable levels to children who recovered from mild infection, however their ability to provide protection against emerging variants may be relatively impaired. Together, these findings indicate that children with MIS-C may develop robust protection from future SARS-CoV-2 infection, an idea consistent with the lack of recurrent MIS-C in previously affected patients (DiLorenzo et al., 2023). In conclusion, our study demonstrates that adaptive immune responses may trigger immunopathology in acute MIS-C, but these same processes may also promote efficacious immune memory. In this way, children may have different mechanisms for responding to and inducing protection to this pandemic virus.

Materials and methods

Human subjects

Pediatric subjects, less than 18 yr of age, were recruited from the New York Presbyterian/Columbia University Irving Medical Center (CUIMC) Morgan Stanley Children's Hospital and pediatric outpatient clinics and divided into cohorts based on their infection history and clinical manifestations: (1) MIS-C: Children followed by the Columbia University Interdisciplinary MIS-C Longitudinal Follow-up Program who met the Center for Disease Control definition of MIS-C; <21 yr of age, fever >38°C for >24 h, laboratory evidence of inflammation, hospital admission, multiorgan involvement, no alternative plausible diagnosis, and positive SARS-CoV-2 serology (Farooqi et al., 2021). All cases were adjudicated by the interdisciplinary team to ensure case definitions were consistent. MIS-C severity was determined by calculation of a vasoactive infusion score, respiratory support requirement, and severity of end organ injury (Jonat et al., 2021). (2) COVID-19: Children requiring hospitalization confirmed to have active SARS-CoV-2 infection by PCR from nasopharyngeal swabs and manifesting with typical symptoms of COVID-19 (fever, malaise, respiratory distress, intestinal involvement) or recruited from the outpatient setting with history of SARS-CoV-2 infection and confirmed to have SARS-CoV-2 antibodies by serologic testing; (3) Seronegative: Subjects with no history of SARS-CoV-2 infection or vaccination and confirmed to not have SARS-CoV-2 antibodies on serologic testing.

Children with documented immunodeficiency, malignancy, or chromosomal abnormalities were excluded from this study. No samples were included following vaccination against SARS-CoV-2. Samples from acute MIS-C and COVID cohorts were obtained within 48 h of hospitalization. 75% of samples in acute MIS-C cohort were obtained prior to or within 12 h of initiation of treatment. Additional samples (up to three total separated by a minimum of 24 h) were obtained from acute COVID subjects during hospitalization and were included only in multivariate analyses. In the MIS-C cohort, no cases of reinfection were noted for those included in longitudinal analyses.

All blood samples were obtained from subjects having routine phlebotomy performed for clinical purposes with informed consent from parents to collect blood for research under a protocol approved by the Institutional Review Board of CUIMC. Serologic testing for anti-SARS-CoV-2 antibodies (anti-S and anti-N immunoglobulins) was performed in the Center for Advanced Laboratory Medicine at CUIMC.

Peripheral blood processing

Blood was processed for the isolation of PBMCs by isolation through density gradient centrifugation using Ficoll-Paque PLUS (GE Healthcare). Mononuclear cells were collected from the buffy coat layer, washed twice with PBS, and resuspended in PBS for analysis.

ELISA for anti-SARS-CoV-2 antibodies

SARS-CoV-2 antibody ELISA was performed as previously described (Amanat et al., 2020). Recombinant S, RBD, and N proteins from a SARS-CoV-2 Wuhan isolate (GenBank: MN908947.3) were purified using the well-established baculovirus expression system as described (Krammer et al., 2012) and generously provided by Dr. Florian Krammer (Mount Sinai School of Medicine, New York, NY, USA). For testing of anti-SARS-CoV-2 antibodies by ELISA, 96-well plates (Immulon 4 HBX; Thermo Fisher Scientific) were coated with recombinant S, RBD, or N protein (2 µg/ml in Dulbecco's PBS [DPBS]) and incubated at 4°C overnight. The next day, antigens were discarded, blocking solution (3% non-fat milk in DPBS with 0.1% Tween 20 [DPBST]) was added for 1 h at room temperature, discarded, and heat-inactivated serum (30 min at 56°C) was added in threefold serial dilutions in DPBST with 1% non-fat milk (starting dilution 1:50) for 2 h at room temperature. Plates were washed with DPBST three times, and then secondary antibodies diluted in DPBST were added. IgG titers were determined using goat anti-human IgG-HRP at 1:3,000 dilution (Thermo Fisher Scientific). IgA titers were determined using anti-human IgA-HRP at 1:10,000 dilution. After washing, secondary antibody solution was added to the plates for 1 h at room temperature. Plates were then washed three times with DPBST before developing with SIGMAFAST o-phenylenediamine dihydrochloride (Sigma-Aldrich) for 10 min. The reaction was subsequently terminated by adding 3 M hydrochloric acid (Sigma-Aldrich), and absorbance at 490 nm (OD_{490}) was measured using a BioTek 800 TS absorbance reader. Values were plotted on dilution curves, and area under the curve (AUC) was calculated using GraphPad Prism software version 9.1.1. For each ELISA run, the mean OD_{490} value of the blank control wells was used to set a background value in the analysis. For display purposes, AUC values below 1 were arbitrarily assigned a value of 0.5.

In vitro T cell stimulation with SARS-CoV-2 peptide MPs

Isolated PBMCs from samples obtained 3–12 mo after infection were isolated fresh and incubated overnight at 37°C in 5% CO_2 following isolation. Cells were stimulated for 6 or 24 h by the addition of SARS-CoV-2–specific megapools (MPs; 1 µg/ml) for $CD4^+$ and $CD8^+$ T cells (MP_S, MP_CD4_R, MP_CD8_A, and MP_CD8_B) designed and synthesized as previously described (Grifoni et al., 2020). Briefly, MP_S consists of 253 15-mer peptides overlapping by 10 residues and covering the entire S protein. MP_CD4_R consists of 221-predicted HLA class II $CD4^+$ T cell epitopes covering all proteins apart from S protein. For $CD8^+$ epitopes, MPs were synthesized based on epitope predictions for 12 most common HLA class I A and B alleles; these resulted in 628 predicted $CD8^+$ T cell epitopes, which were separated into MP_CD8_A and MP_CD8_B (Dan et al., 2021; Grifoni et al., 2020). Immunocult human CD3/CD28 T cell activator (STEMCELL Technologies) was used as a positive control, and equimolar amount of DMSO was used as negative control. Before the addition of peptide MPs, cells were blocked for 15 min with anti-CD40 monoclonal antibody (0.5 µg/ml; Miltenyi Biotec), as previously described (Reiss et al., 2017). After either 6 or 24 h, the supernatant was collected for multiplex detection of cytokines, and cells were stained for AIM and intracellular cytokine production and analyzed via flow cytometry.

AIM^+ antigen-specific $CD4^+$ T cells were identified as positive following Boolean OR gating of the $CD40L^+OX40^+$, $4\text{-}1BB^+OX40^+$,

4-1BB$^+$CD40L$^+$ subsets (see Fig S1 C). The resultant gate was used to quantify AIM$^+$ CD4$^+$ T cell frequency. AIM$^+$ antigen-specific CD8$^+$ T cells were identified as 4-1BB$^+$CD69$^+$. Antigen-specific CD4$^+$ and CD8$^+$ T cells were measured as DMSO background-subtracted data.

Flow cytometry

For flow cytometry analysis of SARS-CoV-2 antigen-reactive T cells and cell sorting, cells were stained in 96-well U-bottom plates protected from light using fluorochrome-conjugated antibodies (see Table S7 for antibodies). Briefly, cells were washed with FACS buffer (PBS with 2% heat-inactivated fetal bovine serum) and then resuspended with surface staining antibody cocktail for 20 min at room temperature. Surface-stained cells were fixed for 30 min at room temperature in fixation buffer (Tonbo), washed with permeabilization buffer (Tonbo), and FACS buffer. Flow cytometry data were collected using the five-laser Cytek Aurora flow cytometer (Cytek Bio) and analyzed using FlowJo v.10.7 software and Graphpad Prism 9.1.1 software.

For flow cytometry analysis of surface markers, cells were stained in polypropylene tubes protected from light using fluorochrome-conjugated antibodies (see Table S7 for antibodies in the T cell flow cytometry panel). Briefly, cells were washed three times with FACS+ buffer (PBS with 5% heat-inactivated fetal bovine serum, 1 mM EDTA) and then resuspended with Zombie NIR Fixable Viability Kit (Biolegend) in 1× PBS for 30 min on ice. Cells were then washed three times with FACS+ buffer then resuspended in TruStain FcX (BioLegend) for 30 min on ice, followed by antibody cocktail in FACS+ buffer for 30 min on ice. Surface-stained cells were then wash three times with FACS + buffer and fixed for 30 min at on ice in BD Cytofix (BD Biosciences). Flow cytometry data were collected using the five-laser Cytek Aurora flow cytometer (Cytek Bio) and analyzed as above. Flow cytometry data was initially gated as in Fig. S1 using FlowJo v.10.7.

TCR sequencing and analysis

CD4$^+$ and CD8$^+$ T cell subsets were isolated by flow cytometry sorting, resuspended in RLT buffer (Qiagen) following sorting, and subsequently frozen at −80°C until DNA extraction. DNA was subsequently extracted from thawed samples using AllPrep DNA/RNA Micro Kit (Qiagen) as per kit instructions. Extracted DNA was resuspended in water and analyzed on NanoDrop2000 spectrophotometer (Thermo Fisher Scientific) to assess DNA quantity and quality confirmed with QubitdsDNA High Sensitivity DNA assay (Thermo Fisher Scientific) prior to sequencing.

TCR Vβ rearrangements were amplified from genomic DNA with two replicates per sample as described (Ritz et al., 2020). Briefly, a cocktail of 23 Vβ families from framework region 2 (FR2) forward primers, and 13 Jβ region reverse primers, modified for NGS from the BIOMED2 primer series (Van Dongen et al., 2003) were used to generate the TRB library and sequenced using an Illumina MiSeq in the Human Immunology Core Facility at the University of Pennsylvania. 2 × 300 bp paired end kits were used for all experiments (Illumina MiSeq Reagent Kit v3, 600 cycle, Illumina Inc.). The sequencing metadata are presented in Table S3. Raw reads were pre-processed using pRESTO (v.0.5.10; Vander Heiden et al., 2014) and clone assemblies were processed with MiXCR (v.2.1.10; Bolotin et al., 2015). Data were analyzed with VDJtools (v.1.2.1; Shugay et al., 2015) and Immunarch (v.0.6.9; Team, 2019) and Prism for visualization and statistics.

CD4$^+$ and CD8$^+$ T cell sorting from peripheral blood

Cryopreserved PBMCs were thawed, washed three times with FACS+ buffer and stained with antibodies indicated in Table S7 in FACS+ buffer for 20 min at room temperature. Cells were washed, filtered, and resuspended in FACS buffer containing 0.01× DNAse. Cells were sorted according to gating strategies outlined in Fig. S1 B using a BD Influx Cell Sorter (BD Biosciences).

RNAseq

Following isolation of CD4$^+$ and CD8$^+$ T cell subsets by FACS, cells were resuspended in RLT Buffer (cat. #1053393; Qiagen) and stored at −80°C until shipment. Frozen RNA samples were sequenced by Genewiz using 150-bp paired end sequencing on an Illumina Hi-Seq. Genewiz provided FASTQ files, Quality control data, and unique hit counts data aligned to the *Homo sapiens* GRCh38 reference genome available on ENSEMBL using the STAR aligner v.2.5.2. The gene list was filtered to exclude any non-coding genes and genes related to hemoglobin function. Next, genes with read counts below five copies in at least five samples were also excluded. DEG analysis was performed and visualized using DESeq2 (Love et al., 2014). Genes were deemed differentially expressed if $\log_2$fold change was ≥1 and adjusted P value ≤0.05. Heatmaps were generated using the pheatmap package (Kolde, 2012), and volcano plots were generated by use of the EnhancedVolcano package. RNAseq data are available at GEO accession number GSE213192.

Multiplex detection of immune mediators

Cryopreserved patient plasma was sent to Eve Technologies Corp. for quantification of human cytokines, chemokines, and growth factors. Cytokine Luminex xMAP technology was used for multiplexed quantification of 71 human cytokines, chemokines, and growth factors: 6CKine, BCA-1, CTACK, EGF, ENA-78, eotaxin, eotaxin-2, eotaxin-3, FGF-2, Flt3L, fractalkine, G-CSF, GM-CSF, GROα, I-309, IFNα2, IFNγ, IL-1α, IL-1β, IL-1RA, IL-2, IL-3, IL-4, IL-5, IL-6, IL-7, IL-8, IL-9, IL-10, IL-12 (p40), IL-12 (p70), IL-13, IL-15, IL-16, IL-17A, IL-17E/IL-25, IL-17F, IL-18, IL-20, IL-21, IL-22, IL-23, IL-27, IL-28, IL-33, IP-10, LIF, MCP-1, MCP-2, MCP-3, MCP-4, M-CSF, MDC, MIG, MIP-1α, MIP-1β, MIP-1δ, PDGF-AA, PDGF-AB/BB, RANTES, sCD40L, SCF, SDF-1α+β, TARC, TGFα, TNFα, TNFβ, TPO, TRAIL, TSLP, and VEGF-A.

The multiplexing analysis was performed using the Luminex 200 system with assay kits sourced by Millipore MILLIPEX (MilliporeSigma) according to the manufacturer's protocol. Observed concentrations were calculated with the standard curve based on the fluorescence intensity of the bead population for a specific analyte. Observed concentrations for each analyte were averaged across every cohort and scaled across cohorts with values ranging from −2 to 2 across all analytes. Heatmap visualizations were generated using the Python data visualization library pheatmap (Kolde, 2012).

Pseudovirus neutralization assay

We used a pseudovirus-based neutralization strategy developed for determination of inhibition of infection and adapted for use with SARS-CoV-2 (Porotto et al., 2009; Talekar et al., 2012; Weisberg et al., 2021). VSV-ΔG-RFP is a recombinant vesicular stomatitis virus (VSV) derived from the cDNA of VSV Indiana, in which the G gene is replaced with the RFP gene. We obtained VSV-ΔG-RFP complemented with VSV-G from Michael Whitt (University of Tennessee Health Science Center, Memphis, TN, USA; and GTX Inc., Memphis, TN, USA). Pseudotyped viruses with the indicated SARS-CoV-2 Spike (S) protein were generated in HEK 293T (human kidney epithelial) cells transfected in poly-D-lysine coated T75 flasks (Corning BioCoat) with 15 µg of DNA, 30 µl of lipofectamine 2000, in 1 ml of Optimem per flask of either the WT (D614G) S (CAD0240757), Delta S (QYJ46503), or Omicron S (UMA71171) cDNAs obtained from Epoch Life Science. 5 h after transfection, the flasks were washed and infected with VSV-ΔG-RFP (multiplicity of infection of 0.5) complemented with VSV-G. Supernatant fluids containing pseudotyped viruses were collected 20 h after infection, centrifuged at 3,000 rpm for 10 min, and immediately used for the neutralization assay. For infection assays, S-pseudotyped virus (50 µl/well, containing 100–400 plaque forming units) from clarified supernatant fluid was used to infect Vero cells (derived from African green monkey kidney, high endogenous expression of ACE2) in 96-well plates pre-filled with 50 µl of media. Fusion-inhibitory peptide corresponding to the HRC domain of S (de Vries et al., 2021) and sera were added at the indicated concentrations. Twofold serial dilutions were performed for all samples. RFP-infected cells were counted using a Cytation 5 (BioTek) and analyzed with Gen5 3.11 software (min object size 25 µm, max object size 135 µm, threshold 3,000).

The sera were tested in three separate experiments performed with technical duplicates in twofold dilutions in 96 well plates. Each plate also contained two controls: (1) immune human serum (IS) subjected to identical dilutions and (2) a fusion inhibitory peptide (HRC_{SARS}; 500, 250, 125, 62.5, 31.25, 15.625, and 7.8125 nM). The measurements from each plate were normalized using the 500 nM concentration of HRC_{SARS} as 100% inhibition and the 1:5,120 dilution of IS as 0% inhibition. The % inhibition was calculated using the following formula: $[1 - (Value_X - HRC_{SARS@500nM}/IS_{@1:5120} - HRC_{SARS@500nM})] \times 100$.

Statistical analysis

Statistical analyses were performed in Prism v.9.1.1, with tests for significance specified in each figure legend. Multiple linear regression analysis was performed on log transformed data with dependent variables (%CD4/CD8 AIM^+; Fig. 7, and antibody AUC/neutralization activity; Fig. 8) including cohort, COVID variant, time from infection (months), and age (years). For each variable, P values were calculated using the *t* statistic with two-sided hypothesis testing.

Online supplementary material

Fig. S1 provides the gating strategy for analytical flow cytometry and sorting. Fig. S2 shows a comparison of surface phenotypic markers between naive and memory subsets and analysis of T cell marker expression in paired samples from subjects during acute MIS-C and following recovery. Fig. S3 includes antibody titer results of SARS-CoV-2–specific antibodies in children with MIS-C during acute disease and following recovery grouped by initial disease severity in longitudinal samples up to 19 mo following initial MIS-C hospitalization. The supplemental tables include DEG analysis comparing T cells in acute MIS-C to recovery in Table S1 ($CD4^+$ T cells) and Table S2 ($CD8^+$ T cells). Table S3 contains TCR sequencing metadata. Multivariate analyses are located in Table S4 (SARS-CoV-2 activation–induced marker assay), Table S5 (anti-SARS-CoV-2 antibody), and Table S6 (neutralization assay). Table S7 contains a list of antibodies used for flow cytometry experiments.

Data availability

Data related to RNAseq is available at GEO accession no. GSE213192. Further information and requests for data or reagents should be directed to and will be fulfilled by lead author Donna L. Farber (df2396@cumc.columbia.edu).

Acknowledgments

The authors wish to thank Shivali Verma for help with the RNAseq analysis, Steven Wells for help with the flow cytometry data, and Carlos Aguilar-Breton, Yannett Franklin, and Chantal Sanchez for help with subject recruitment and clinical data management. We acknowledge Dr. Peter Dayan and Dr. Mark Gorelik for their coordination and identification of subjects with MIS-C. We also acknowledge the faculty and staff of the Morgan Stanley Children's Hospital of New York, New York Presbyterian Hospital, and the Columbia University Interdisciplinary MIS-C Longitudinal Follow-up Program for their clinical service and their efforts in collecting samples. Biospecimens utilized for this research were in part obtained from the Columbia University Biobank. We thank Dr. Florian Kramer (Mt. Sinai School of Medicine) for providing the reagent for the SARS-CoV-2 ELISA. We are grateful to the parents and patients who generously provided samples for our study. Graphical abstract created with BioRender.com.

This study was supported by National Institutes of Health (NIH) grants AI100119 and AI168634, awarded to D.L. Farber. T.J. Connors was supported by NIH grant AI141686. J. Davis-Porada was supported by NIH grant T32GM145440-01. NIH grants S10OD020056 and S10OD030282 were awarded to the Columbia Flow Cytometry Core. The Columbia University Biobank is supported by the Irving Institute for Clinical and Translational Research, home to Columbia University's Clinical and Translational Science Award, funded through grant no. UL1TR001873 from the National Center for Advancing Translational Sciences/NIH, and support to the Human Immunology Core facility at the University of Pennsylvania from NIH grants 2P30AI1045008 and 2P30CA016520.

Author contributions: Conceptualization: T.J. Connors and D.L. Farber. Data curation: K. Rybkina. Formal analysis: K. Rybkina, J.N. Bell, T. Wohlbold, M.C. Bradley, M. Scafuro, W. Meng, M. Porotto, E.T. Luning Prak, and T.J. Connors. Funding acquisition: D.L. Farber. Investigation: K. Rybkina, J.N. Bell,

T. Wohlbold, M.C. Bradley, M. Scafuro, W. Meng, B.R. Anderson, R.J. Weller, J.D. Milner, R.C. Korenberg, J. Davis-Porada, A. Moscona, M. Porotto, E.T. Luning Prak, K. Pethe, and T.J. Connors. Methodology: K. Rybkina, A. Moscona, M. Porotto, E.T. Luning Prak, T.J. Connors, and D.L. Farber. Project administration: D L. Farber. Supervision: T.J. Connors, D.L. Farber, A. Moscona, and M. Porotto. Visualization: K. Rybkina, J.N. Bell, T.J. Connors, and D.L. Farber. Writing—original draft: K. Rybkina, T.J. Connors, and D.L. Farber. Writing—review & editing: all authors.

Disclosures: B.R. Anderson reported grants from Genentech and the National Institutes of Health outside the submitted work. J. Milner reported personal fees from Blueprint Medicines outside the submitted work. T.J. Connors reported grants from the National Institutes of Health during the conduct of the study and outside the submitted work. No other disclosures were reported.

Submitted: 1 September 2022
Revised: 9 February 2023
Accepted: 7 April 2023

References

Amanat, F., D. Stadlbauer, S. Strohmeier, T.H.O. Nguyen, V. Chromikova, M. McMahon, K. Jiang, G.A. Arunkumar, D. Jurczyszak, J. Polanco, et al. 2020. A serological assay to detect SARS-CoV-2 seroconversion in humans. *Nat. Med.* 26:1033–1036. https://doi.org/10.1038/s41591-020-0913-5

Bajaj, R., H.C. Sinclair, K. Patel, B. Low, A. Pericao, C. Manisty, O. Guttmann, F. Zemrak, O. Miller, P. Longhi, et al. 2021. Delayed-onset myocarditis following COVID-19. *Lancet Respir. Med.* 9:e32–e34. https://doi.org/10.1016/S2213-2600(21)00085-0

Becker, Y. 2006. Respiratory syncytial virus (RSV) evades the human adaptive immune system by skewing the Th1/Th2 cytokine balance toward increased levels of Th2 cytokines and IgE, markers of allergy: A review. *Virus Genes.* 33:235–252. https://doi.org/10.1007/s11262-006-0064-x

Belhadjer, Z., J. Auriau, M. Méot, M. Oualha, S. Renolleau, L. Houyel, and D. Bonnet. 2020. Addition of corticosteroids to immunoglobulins is associated with recovery of cardiac function in multi-inflammatory syndrome in children. *Circulation.* 142:2282–2284. https://doi.org/10.1161/CIRCULATIONAHA.120.050147

Bolotin, D.A., S. Poslavsky, I. Mitrophanov, M. Shugay, I.Z. Mamedov, E.V. Putintseva, and D.M. Chudakov. 2015. MiXCR: Software for comprehensive adaptive immunity profiling. *Nat. Methods.* 12:380–381. https://doi.org/10.1038/nmeth.3364

Bonecchi, R., F. Facchetti, S. Dusi, W. Luini, D. Lissandrini, M. Simmelink, M. Locati, S. Bernasconi, P. Allavena, E. Brandt, et al. 2000. Induction of functional IL-8 receptors by IL-4 and IL-13 in human monocytes. *J. Immunol.* 164:3862–3869. https://doi.org/10.4049/jimmunol.164.7.3862

Burbelo, P.D., R. Castagnoli, C. Shimizu, O.M. Delmonte, K. Dobbs, V. Discepolo, A. Lo Vecchio, A. Guarino, F. Licciardi, U. Ramenghi, et al. 2022. Autoantibodies against proteins previously associated with autoimmunity in adult and pediatric patients with COVID-19 and children with MIS-C. *Front. Immunol.* 13:841126. https://doi.org/10.3389/fimmu.2022.841126

Carter, M.J., M. Fish, A. Jennings, K.J. Doores, P. Wellman, J. Seow, S. Acors, C. Graham, E. Timms, J. Kenny, et al. 2020. Peripheral immunophenotypes in children with multisystem inflammatory syndrome associated with SARS-CoV-2 infection. *Nat. Med.* 26:1701–1707. https://doi.org/10.1038/s41591-020-1054-6

Chen, Y., J. Shen, M.Y. Kasmani, P. Topchyan, and W. Cui. 2021. Single-cell transcriptomics reveals Core regulatory programs that determine the heterogeneity of circulating and tissue-resident memory CD8$^+$ T cells. *Cells.* 10:2143. https://doi.org/10.3390/cells10082143

Cheng, M.H., S. Zhang, R.A. Porritt, M. Noval Rivas, L. Paschold, E. Willscher, M. Binder, M. Arditi, and I. Bahar. 2020. Superantigenic character of an insert unique to SARS-CoV-2 spike supported by skewed TCR repertoire in patients with hyperinflammation. *Proc. Natl. Acad. Sci. USA.* 117:25254–25262. https://doi.org/10.1073/pnas.2010722117

Cheung, E.W., P. Zachariah, M. Gorelik, A. Boneparth, S.G. Kernie, J.S. Orange, and J.D. Milner. 2020. Multisystem inflammatory syndrome related to COVID-19 in previously healthy children and adolescents in New York city. *JAMA.* 324:294–296. https://doi.org/10.1001/jama.2020.10374

Cloete, J., A. Kruger, M. Masha, N.M. du Plessis, D. Mawela, M. Tshukudu, T. Manyane, L. Komane, M. Venter, W. Jassat, et al. 2022. Paediatric hospitalisations due to COVID-19 during the first SARS-CoV-2 omicron (B.1.1.529) variant wave in South Africa: A multicentre observational study. *Lancet Child Adolesc. Health.* 6:294–302. https://doi.org/10.1016/S2352-4642(22)00027-X

Consiglio, C.R., N. Cotugno, F. Sardh, C. Pou, D. Amodio, L. Rodriguez, Z. Tan, S. Zicari, A. Ruggiero, G.R. Pascucci, et al. 2020. The Immunology of multisystem inflammatory syndrome in children with COVID-19. *Cell.* 183:968–981.e7. https://doi.org/10.1016/j.cell.2020.09.016

Conway, S.R., C.A. Lazarski, N.E. Field, M. Jensen-Wachspress, H. Lang, V. Kankate, J. Durkee-Shock, H. Kinoshita, W. Suslovic, K. Webber, et al. 2022. SARS-CoV-2-Specific T cell responses are stronger in children with multisystem inflammatory syndrome compared to children with uncomplicated SARS-CoV-2 infection. *Front. Immunol.* 12:793197. https://doi.org/10.3389/fimmu.2021.793197

Crosby, L., S. Balasubramanian, and A.V. Ramanan. 2021. Steroids or intravenous immunoglobulin as first line in MIS-C in LMICs. *Lancet Rheumatol.* 3:e615–e616. https://doi.org/10.1016/S2665-9913(21)00223-X

Crotty, S. 2011. Follicular helper CD4 T cells (TFH). *Annu. Rev. Immunol.* 29:621–663. https://doi.org/10.1146/annurev-immunol-031210-101400

Dan, J.M., J. Mateus, Y. Kato, K.M. Hastie, E.D. Yu, C.E. Faliti, A. Grifoni, S.I. Ramirez, S. Haupt, A. Frazier, et al. 2021. Immunological memory to SARS-CoV-2 assessed for up to 8 months after infection. *Science.* 371:eabf4063 https://doi.org/10.1126/science.abf4063

de Vries, R.D., K.S. Schmitz, F.T. Bovier, C. Predella, J. Khao, D. Noack, B.L. Haagmans, S. Herfst, K.N. Stearns, J. Drew-Bear, et al. 2021. Intranasal fusion inhibitory lipopeptide prevents direct-contact SARS-CoV-2 transmission in ferrets. *Science.* 371:1379–1382. https://doi.org/10.1126/science.abf4896

DiLorenzo, M.P., K.M. Farooqi, A.M. Shah, A. Channing, J.K. Harrington, T.J. Connors, K. Martirosyan, U.S. Krishnan, A. Ferris, R.J. Weller, et al. 2023. Ventricular function and tissue characterization by cardiac magnetic resonance imaging following hospitalization for multisystem inflammatory syndrome in children: A prospective study. *Pediatr. Radiol.* 53:394–403. https://doi.org/10.1007/s00247-022-05521-5

Diorio, C., S.E. Henrickson, L.A. Vella, K.O. McNerney, J. Chase, C. Burudpakdee, J.H. Lee, C. Jasen, F. Balamuth, D.M. Barrett, et al. 2020. Multisystem inflammatory syndrome in children and COVID-19 are distinct presentations of SARS-CoV-2. *J. Clin. Invest.* 130:5967–5975. https://doi.org/10.1172/JCI140970

Evans, J.P., C. Zeng, C. Carlin, G. Lozanski, L.J. Saif, E.M. Oltz, R.J. Gumina, and S.L. Liu. 2022. Neutralizing antibody responses elicited by SARS-CoV-2 mRNA vaccination wane over time and are boosted by breakthrough infection. *Sci. Transl. Med.* 14:eabn8057. https://doi.org/10.1126/scitranslmed.abn8057

Farooqi, K.M., A. Chan, R.J. Weller, J. Mi, P. Jiang, E. Abrahams, A. Ferris, U.S. Krishnan, N. Pasumarti, S. Suh, et al. 2021. Longitudinal outcomes for multisystem inflammatory syndrome in children. *Pediatrics.* 148:e2021051155. https://doi.org/10.1542/peds.2021-051155

Feldstein, L.R., E.B. Rose, S.M. Horwitz, J.P. Collins, M.M. Newhams, M.B.F. Son, J.W. Newburger, L.C. Kleinman, S.M. Heidemann, A.A. Martin, et al. 2020. Multisystem inflammatory syndrome in U.S. Children and adolescents. *N. Engl. J. Med.* 383:334–346. https://doi.org/10.1056/NEJMoa2021680

Grifoni, A., D. Weiskopf, S.I. Ramirez, J. Mateus, J.M. Dan, C.R. Moderbacher, S.A. Rawlings, A. Sutherland, L. Premkumar, R.S. Jadi, et al. 2020. Targets of T Cell responses to SARS-CoV-2 coronavirus in humans with COVID-19 disease and unexposed individuals. *Cell.* 181:1489–1501.e15. https://doi.org/10.1016/j.cell.2020.05.015

Gruber, C.N., R.S. Patel, R. Trachtman, L. Lepow, F. Amanat, F. Krammer, K.M. Wilson, K. Onel, D. Geanon, K. Tuballes, et al. 2020. Mapping systemic inflammation and antibody responses in multisystem inflammatory syndrome in children (MIS-C). *Cell.* 183:982–995.e14. https://doi.org/10.1016/j.cell.2020.09.034

Hadjadj, J., N. Yatim, L. Barnabei, A. Corneau, J. Boussier, N. Smith, H. Péré, B. Charbit, V. Bondet, C. Chenevier-Gobeaux, et al. 2020. Impaired type

I interferon activity and inflammatory responses in severe COVID-19 patients. *Science*. 369:718–724. https://doi.org/10.1126/science.abc6027

Hoste, L., L. Roels, L. Naesens, V. Bosteels, S. Vanhee, S. Dupont, C. Bosteels, R. Browaeys, N. Vandamme, K. Verstaen, et al. 2022. TIM3+ TRBV11-2 T cells and IFNγ signature in patrolling monocytes and CD16+ NK cells delineate MIS-C. *J. Exp. Med.* 219:e20211381. https://doi.org/10.1084/jem.20211381

Hsieh, L.E., J. Song, A. Grifoni, C. Shimizu, A.H. Tremoulet, K.B. Dummer, J.C. Burns, A. Sette, and A. Franco. 2022. T cells in multisystem inflammatory syndrome in children (MIS-C) have a predominant CD4+ T helper response to SARS-CoV-2 peptides and numerous virus-specific CD4- CD8- double-negative T cells. *Int. J. Mol. Sci.* 23:7219. https://doi.org/10.3390/ijms23137219

Jonat, B., M. Gorelik, A. Boneparth, A.S. Geneslaw, P. Zachariah, A. Shah, L. Broglie, J. Duran, K.D. Morel, M. Zorrilla, et al. 2021. Multisystem inflammatory syndrome in children associated with coronavirus disease 2019 in a Children's hospital in New York city: Patient characteristics and an institutional protocol for evaluation, management, and follow-up. *Pediatr. Crit. Care Med.* 22:e178–e191. https://doi.org/10.1097/PCC.0000000000002598

Kolde, R. 2012. Pheatmap: Pretty heatmaps. *R package version*. 1:726

Krammer, F., I. Margine, G.S. Tan, N. Pica, J.C. Krause, and P. Palese. 2012. A carboxy-terminal trimerization domain stabilizes conformational epitopes on the stalk domain of soluble recombinant hemagglutinin substrates. *PLoS One*. 7:e43603. https://doi.org/10.1371/journal.pone.0043603

Kumar, B.V., W. Ma, M. Miron, T. Granot, R.S. Guyer, D.J. Carpenter, T. Senda, X. Sun, S.H. Ho, H. Lerner, et al. 2017. Human tissue-resident memory T cells are defined by Core transcriptional and functional signatures in lymphoid and mucosal sites. *Cell Rep.* 20:2921–2934. https://doi.org/10.1016/j.celrep.2017.08.078

Lam, K.P., M. Chiñas, A.M. Julé, M. Taylor, M. Ohashi, M. Benamar, E. Crestani, M.B.F. Son, J. Chou, C. Gebhart, et al. 2022. SARS-CoV-2-specific T cell responses in patients with multisystem inflammatory syndrome in children. *Clin. Immunol.* 243:109106. https://doi.org/10.1016/j.clim.2022.109106

Lee, P.Y., M. Day-Lewis, L.A. Henderson, K.G. Friedman, J. Lo, J.E. Roberts, M.S. Lo, C.D. Platt, J. Chou, K.J. Hoyt, et al. 2020. Distinct clinical and immunological features of SARS-CoV-2-induced multisystem inflammatory syndrome in children. *J. Clin. Invest.* 130:5942–5950. https://doi.org/10.1172/JCI141113

Love, M.I., W. Huber, and S. Anders. 2014. Moderated estimation of fold change and dispersion for RNA-seq data with DESeq2. *Genome Biol.* 15:550. https://doi.org/10.1186/s13059-014-0550-8

Low, D.E. 2013. Toxic shock syndrome: Major advances in pathogenesis, but not treatment. *Crit. Care Clin.* 29:651–675. https://doi.org/10.1016/j.ccc.2013.03.012

Lu, X., L. Zhang, H. Du, J. Zhang, Y.Y. Li, J. Qu, W. Zhang, Y. Wang, S. Bao, Y. Li, et al. 2020. SARS-CoV-2 infection in children. *N. Engl. J. Med.* 382:1663–1665. https://doi.org/10.1056/NEJMc2005073

Lucas, C., P. Wong, J. Klein, T.B.R. Castro, J. Silva, M. Sundaram, M.K. Ellingson, T. Mao, J.E. Oh, B. Israelow, et al. 2020. Longitudinal analyses reveal immunological misfiring in severe COVID-19. *Nature*. 584:463–469. https://doi.org/10.1038/s41586-020-2588-y

Mackay, L.K., M. Minnich, N.A. Kragten, Y. Liao, B. Nota, C. Seillet, A. Zaid, K. Man, S. Preston, D. Freestone, et al. 2016. Hobit and Blimp1 instruct a universal transcriptional program of tissue residency in lymphocytes. *Science*. 352:459–463. https://doi.org/10.1126/science.aad2035

Martin, B., P.E. DeWitt, S. Russell, A. Anand, K.R. Bradwell, C. Bremer, D. Gabriel, A.T. Girvin, J.G. Hajagos, J.A. McMurry, et al. 2022. Characteristics, outcomes, and severity risk factors associated with SARS-CoV-2 infection among children in the US national COVID cohort collaborative. *JAMA Netw. Open*. 5:e2143151. https://doi.org/10.1001/jamanetworkopen.2021.43151

Matsubara, D., J. Chang, H.L. Kauffman, Y. Wang, S. Nadaraj, C. Patel, S.M. Paridon, M.A. Fogel, M.D. Quartermain, and A. Banerjee. 2022. Longitudinal assessment of cardiac outcomes of multisystem inflammatory syndrome in children associated with COVID-19 infections. *J. Am. Heart Assoc.* 11:e023251. https://doi.org/10.1161/JAHA.121.023251

Miesbach, W. 2020. Pathological role of angiotensin II in severe COVID-19. *TH Open*. 4:e138–e144. https://doi.org/10.1055/s-0040-1713678

Miron, M., W. Meng, A.M. Rosenfeld, S. Dvorkin, M.M.L. Poon, N. Lam, B.V. Kumar, Y. Louzoun, E.T. Luning Prak, and D.L. Farber. 2021. Maintenance of the human memory T cell repertoire by subset and tissue site. *Genome Med.* 13:100. https://doi.org/10.1186/s13073-021-00918-7

Moreews, M., K. Le Gouge, S. Khaldi-Plassart, R. Pescarmona, A.L. Mathieu, C. Malcus, S. Djebali, A. Bellomo, O. Dauwalder, M. Perret, et al. 2021. Polyclonal expansion of TCR Vbeta 21.3(+) CD4(+) and CD8(+) T cells is a hallmark of Multisystem Inflammatory Syndrome in Children. *Sci Immunol*. 6:eabh1516. https://doi.org/10.1126/sciimmunol.abh1516

Newton, A.H., A. Cardani, and T.J. Braciale. 2016. The host immune response in respiratory virus infection: Balancing virus clearance and immunopathology. *Semin. Immunopathol.* 38:471–482. https://doi.org/10.1007/s00281-016-0558-0

Norlander, A.E., M.A. Saleh, A.K. Pandey, H.A. Itani, J. Wu, L. Xiao, J. Kang, B.L. Dale, S.B. Goleva, F. Laroumanie, et al. 2017. A salt-sensing kinase in T lymphocytes, SGK1, drives hypertension and hypertensive end-organ damage. *JCI Insight*. 2:e92801. https://doi.org/10.1172/jci.insight.92801

Noval Rivas, M., R.A. Porritt, M.H. Cheng, I. Bahar, and M. Arditi. 2021. COVID-19-associated multisystem inflammatory syndrome in children (MIS-C): A novel disease that mimics toxic shock syndrome-the superantigen hypothesis. *J. Allergy Clin. Immunol.* 147:57–59. https://doi.org/10.1016/j.jaci.2020.10.008

Noval Rivas, M., R.A. Porritt, M.H. Cheng, I. Bahar, and M. Arditi. 2022. Multisystem inflammatory syndrome in children and long COVID: The SARS-CoV-2 viral superantigen hypothesis. *Front. Immunol.* 13:941009. https://doi.org/10.3389/fimmu.2022.941009

Parri, N., M. Lenge, and D. Buonsenso, and Coronavirus Infection in Pediatric Emergency Departments (CONFIDENCE) Research Group. 2020. Children with covid-19 in pediatric emergency departments in Italy. *N. Engl. J. Med.* 383:187–190. https://doi.org/10.1056/NEJMc2007617

Pierce, C.A., P. Preston-Hurlburt, Y. Dai, C.B. Aschner, N. Cheshenko, B. Galen, S.J. Garforth, N.G. Herrera, R.K. Jangra, N.C. Morano, et al. 2020. Immune responses to SARS-CoV-2 infection in hospitalized pediatric and adult patients. *Sci. Transl. Med.* 12. eabd5487. https://doi.org/10.1126/scitranslmed.abd5487

Pope, S.M., E.B. Brandt, A. Mishra, S.P. Hogan, N. Zimmermann, K.I. Matthaei, P.S. Foster, and M.E. Rothenberg. 2001. IL-13 induces eosinophil recruitment into the lung by an IL-5- and eotaxin-dependent mechanism. *J. Allergy Clin. Immunol.* 108:594–601. https://doi.org/10.1067/mai.2001.118600

Porotto, M., G. Orefice, C.C. Yokoyama, B.A. Mungall, R. Realubit, M.L. Sganga, M. Aljofan, M. Whitt, F. Glickman, and A. Moscona. 2009. Simulating henipavirus multicycle replication in a screening assay leads to identification of a promising candidate for therapy. *J. Virol.* 83:5148–5155. https://doi.org/10.1128/JVI.00164-09

Porritt, R.A., A. Binek, L. Paschold, M.N. Rivas, A. McArdle, L.M. Yonker, G. Alter, H.K. Chandnani, M. Lopez, A. Fasano, et al. 2021a. The autoimmune signature of hyperinflammatory multisystem inflammatory syndrome in children. *J. Clin. Invest.* 131:e151520. https://doi.org/10.1172/JCI151520

Porritt, R.A., L. Paschold, M.N. Rivas, M.H. Cheng, L.M. Yonker, H. Chandnani, M. Lopez, D. Simnica, C. Schultheiß, C. Santiskulvong, et al. 2021b. HLA class I-associated expansion of TRBV11-2 T cells in multisystem inflammatory syndrome in children. *J. Clin. Invest.* 131:e146614. https://doi.org/10.1172/JCI146614

Ramaswamy, A., N.N. Brodsky, T.S. Sumida, M. Comi, H. Asashima, K.B. Hoehn, N. Li, Y. Liu, A. Shah, N.G. Ravindra, et al. 2021. Immune dysregulation and autoreactivity correlate with disease severity in SARS-CoV-2-associated multisystem inflammatory syndrome in children. *Immunity*. 54:1083–1095.e7. https://doi.org/10.1016/j.immuni.2021.04.003

Ravichandran, S., J. Tang, G. Grubbs, Y. Lee, S. Pourhashemi, L. Hussaini, S.A. Lapp, R.C. Jerris, V. Singh, A. Chahroudi, et al. 2021. SARS-CoV-2 immune repertoire in MIS-C and pediatric COVID-19. *Nat. Immunol.* 22:1452–1464. https://doi.org/10.1038/s41590-021-01051-8

Reilly, E.C., K. Lambert Emo, P.M. Buckley, N.S. Reilly, I. Smith, F.A. Chaves, H. Yang, P.W. Oakes, and D.J. Topham. 2020. T_{RM} integrins CD103 and CD49a differentially support adherence and motility after resolution of influenza virus infection. *Proc. Natl. Acad. Sci. USA*. 117:12306–12314. https://doi.org/10.1073/pnas.1915681117

Reiss, S., A.E. Baxter, K.M. Cirelli, J.M. Dan, A. Morou, A. Daigneault, N. Brassard, G. Silvestri, J.-P. Routy, C. Havenar-Daughton, et al. 2017. Comparative analysis of activation induced marker (AIM) assays for sensitive identification of antigen-specific CD4 T cells. *PLoS One*. 12:e0186998. https://doi.org/10.1371/journal.pone.0186998

Riphagen, S., X. Gomez, C. Gonzalez-Martinez, N. Wilkinson, and P. Theocharis. 2020. Hyperinflammatory shock in children during COVID-19 pandemic. *Lancet*. 395:1607–1608. https://doi.org/10.1016/S0140-6736(20)31094-1

Ritz, C., W. Meng, N.L. Stanley, M.L. Baroja, C. Xu, P. Yan, A.C. Huang, R. Hausler, P. Nicholas, J.-M. Fan, et al. 2020. Postvaccination graft dysfunction/aplastic anemia relapse with massive clonal expansion of autologous CD8+ lymphocytes. *Blood Adv.* 4:1378–1382. https://doi.org/10.1182/bloodadvances.2019000853

Rodriguez-Smith, J.J., E.L. Verweyen, G.M. Clay, Y.M. Esteban, S.R. de Loizaga, E.J. Baker, T. Do, S. Dhakal, S.M. Lang, A.A. Grom, et al. 2021. Inflammatory biomarkers in COVID-19-associated multisystem inflammatory syndrome in children, Kawasaki disease, and macrophage activation syndrome: A cohort study. *Lancet Rheumatol.* 3:e574–e584. https://doi.org/10.1016/S2665-9913(21)00139-9

Rojas, J.M., M. Avia, V. Martín, and N. Sevilla. 2017. IL-10: A multifunctional cytokine in viral infections. *J. Immunol. Res.* 2017:6104054. https://doi.org/10.1155/2017/6104054

Sacco, K., R. Castagnoli, S. Vakkilainen, C. Liu, O.M. Delmonte, C. Oguz, I.M. Kaplan, S. Alehashemi, P.D. Burbelo, F. Bhuyan, et al. 2022. Immunopathological signatures in multisystem inflammatory syndrome in children and pediatric COVID-19. *Nat. Med.* 28:1050–1062. https://doi.org/10.1038/s41591-022-01724-3

Schmidt, F., F. Muecksch, Y. Weisblum, J. Da Silva, E. Bednarski, A. Cho, Z. Wang, C. Gaebler, M. Caskey, M.C. Nussenzweig, et al. 2022. Plasma neutralization of the SARS-CoV-2 omicron variant. *N. Engl. J. Med.* 386: 599–601. https://doi.org/10.1056/NEJMc2119641

Sharma, C., M. Ganigara, C. Galeotti, J. Burns, F.M. Berganza, D.A. Hayes, D. Singh-Grewal, S. Bharath, S. Sajjan, and J. Bayry. 2021. Multisystem inflammatory syndrome in children and Kawasaki disease: A critical comparison. *Nat. Rev. Rheumatol.* 17:731–748. https://doi.org/10.1038/s41584-021-00709-9

Shugay, M., D.V. Bagaev, M.A. Turchaninova, D.A. Bolotin, O.V. Britanova, E.V. Putintseva, M.V. Pogorelyy, V.I. Nazarov, I.V. Zvyagin, V.I. Kirgizova, et al. 2015. VDJtools: Unifying post-analysis of T cell receptor repertoires. *PLOS Comput. Biol.* 11:e1004503. https://doi.org/10.1371/journal.pcbi.1004503

Stelitano, D., S.P. Weisberg, M.P. Goldklang, Y. Zhu, F.T. Bovier, G.F. Kalantarov, G. Greco, D. Decimo, G. Franci, M. Cennamo, et al. 2021. Rapid and flexible platform to assess anti-SARS-CoV-2 antibody neutralization and spike protein-specific antivirals. *MSphere*. 6:e0057121. https://doi.org/10.1128/mSphere.00571-21

Sun, J., R. Madan, C.L. Karp, and T.J. Braciale. 2009. Effector T cells control lung inflammation during acute influenza virus infection by producing IL-10. *Nat. Med.* 15:277–284. https://doi.org/10.1038/nm.1929

Szabo, P.A., P. Dogra, J.I. Gray, S.B. Wells, T.J. Connors, S.P. Weisberg, I. Krupska, R. Matsumoto, M.M.L. Poon, E. Idzikowski, et al. 2021. Longitudinal profiling of respiratory and systemic immune responses reveals myeloid cell-driven lung inflammation in severe COVID-19. *Immunity*. 54:797–814.e6. https://doi.org/10.1016/j.immuni.2021.03.005

Szabo, P.A., H.M. Levitin, M. Miron, M.E. Snyder, T. Senda, J. Yuan, Y.L. Cheng, E.C. Bush, P. Dogra, P. Thapa, et al. 2019a. Single-cell transcriptomics of human T cells reveals tissue and activation signatures in health and disease. *Nat. Commun.* 10:4706. https://doi.org/10.1038/s41467-019-12464-3

Szabo, P.A., M. Miron, and D.L. Farber. 2019b. Location, location, location: Tissue resident memory T cells in mice and humans. *Sci. Immunol.* 4: eaas9673. https://doi.org/10.1126/sciimmunol.aas9673

Talekar, A., A. Pessi, F. Glickman, U. Sengupta, T. Briese, M.A. Whitt, C. Mathieu, B. Horvat, A. Moscona, and M. Porotto. 2012. Rapid screening for entry inhibitors of highly pathogenic viruses under low-level biocontainment. *PLoS One*. 7:e30538. https://doi.org/10.1371/journal.pone.0030538

Team, I. 2019. Immunarch: An R package for painless bioinformatics analysis of T-cell and B-cell immune repertoires. *Zenodo*. 10. https://doi.org/10.5281/zenodo.3367200

van Dongen, J.J.M., A.W. Langerak, M. Brüggemann, P.A.S. Evans, M. Hummel, F.L. Lavender, E. Delabesse, F. Davi, E. Schuuring, R. García-Sanz, et al. 2003. Design and standardization of PCR primers and protocols for detection of clonal immunoglobulin and T-cell receptor gene recombinations in suspect lymphoproliferations: Report of the BIOMED-2 concerted action BMH4-CT98-3936. *Leukemia*. 17:2257–2317. https://doi.org/10.1038/sj.leu.2403202

Vander Heiden, J.A., G. Yaari, M. Uduman, J.N. Stern, K.C. O'Connor, D.A. Hafler, F. Vigneault, and S.H. Kleinstein. 2014. pRESTO: A toolkit for processing high-throughput sequencing raw reads of lymphocyte receptor repertoires. *Bioinformatics*. 30:1930–1932. https://doi.org/10.1093/bioinformatics/btu138

Vella, L.A., J.R. Giles, A.E. Baxter, D.A. Oldridge, C. Diorio, L. Kuri-Cervantes, C. Alanio, M.B. Pampena, J.E. Wu, Z. Chen, et al. 2021. Deep immune profiling of MIS-C demonstrates marked but transient immune activation compared to adult and pediatric COVID-19. *Sci. Immunol.* 6: eabf7570. https://doi.org/10.1126/sciimmunol.abf7570

Verdoni, L., A. Mazza, A. Gervasoni, L. Martelli, M. Ruggeri, M. Ciuffreda, E. Bonanomi, and L. D'Antiga. 2020. An outbreak of severe kawasaki-like disease at the Italian epicentre of the SARS-CoV-2 epidemic: An observational cohort study. *Lancet*. 395:1771–1778. https://doi.org/10.1016/S0140-6736(20)31103-X

Wang, L., N.A. Berger, D.C. Kaelber, P.B. Davis, N.D. Volkow, and R. Xu. 2022. Incidence rates and clinical outcomes of SARS-CoV-2 infection with the omicron and delta variants in children younger than 5 Years in the US. *JAMA Pediatr.* 176:811–813. https://doi.org/10.1001/jamapediatrics.2022.0945

Weisberg, S.P., T.J. Connors, Y. Zhu, M.R. Baldwin, W.H. Lin, S. Wontakal, P.A. Szabo, S.B. Wells, P. Dogra, J. Gray, et al. 2021. Distinct antibody responses to SARS-CoV-2 in children and adults across the COVID-19 clinical spectrum. *Nat. Immunol.* 22:25–31. https://doi.org/10.1038/s41590-020-00826-9

Wherry, E.J. 2011. T cell exhaustion. *Nat. Immunol.* 12:492–499. https://doi.org/10.1038/ni.2035

Yonker, L.M., T. Gilboa, A.F. Ogata, Y. Senussi, R. Lazarovits, B.P. Boribong, Y.C. Bartsch, M. Loiselle, M.N. Rivas, R.A. Porritt, et al. 2021. Multisystem inflammatory syndrome in children is driven by zonulin-dependent loss of gut mucosal barrier. *J. Clin. Invest.* 131:e149633. https://doi.org/10.1172/JCI149633

Yuan, X.H., Y.M. Li, Y.Y. Shen, J. Yang, and Y. Jin. 2020. Clinical and Th1/Th2 immune response features of hospitalized children with human rhinovirus infection. *J. Med. Virol.* 92:26–33. https://doi.org/10.1002/jmv.25587

JEM

Supplemental material

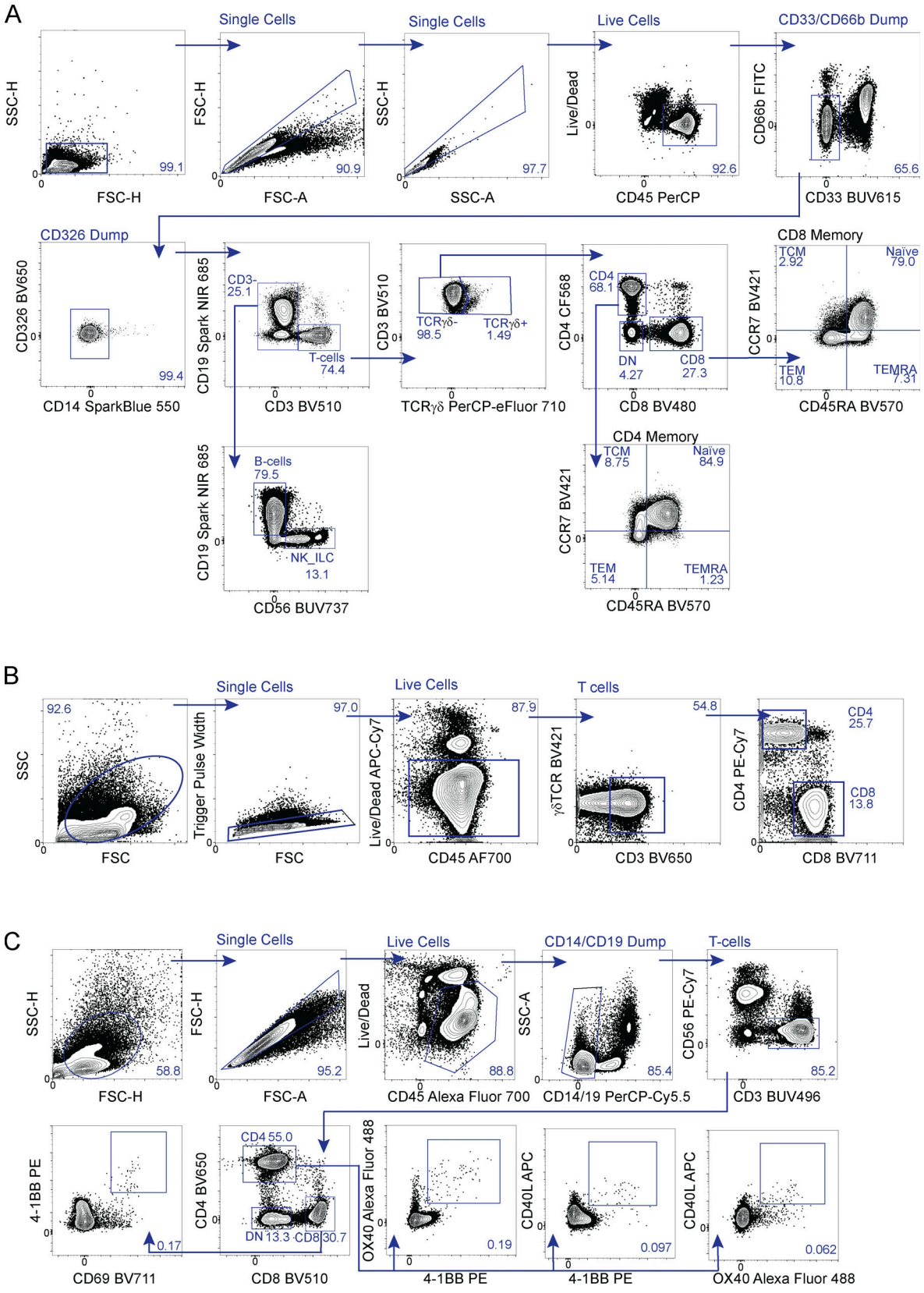

Figure S1. **Gating strategy for flow cytometry and cell sorting. (A)** Gating strategy for blood immunophenotyping. **(B)**. Gating strategy used for cell sorting for RNAseq. **(C)** Gating strategy for identification of SARS-CoV-2–specific T cells. Numbers on flow cytometry plots represent % of cells within gate. FSC, forward scatter; SSC, side scatter.

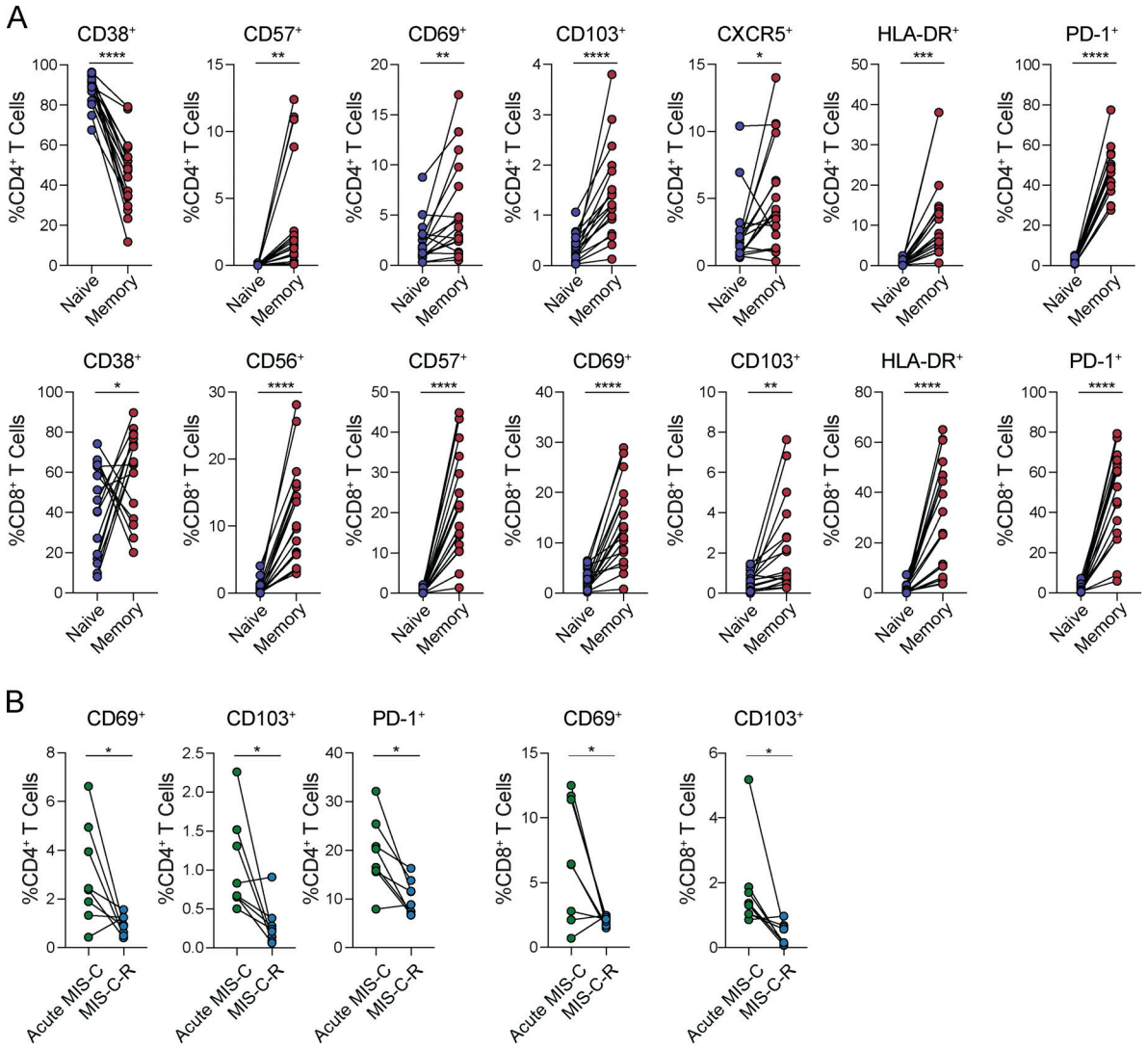

Figure S2. **Expression of activation and tissue residency markers on T cells during acute MIS-C are absent in recovery. (A)** Paired analysis of marker expression on naive and memory CD4+ (top) and CD8+ (bottom) T cells during acute MIS-C (n = 17). **(B)**. Paired analysis of marker expression on CD4+ (left) and CD8+ (right) T cells during acute MIS-C and following recovery (n = 8). Statistical analyses were performed using paired t test. *, P < 0.05; **, P < 0.01; ***, P < 0.001; ****, P < 0.0001.

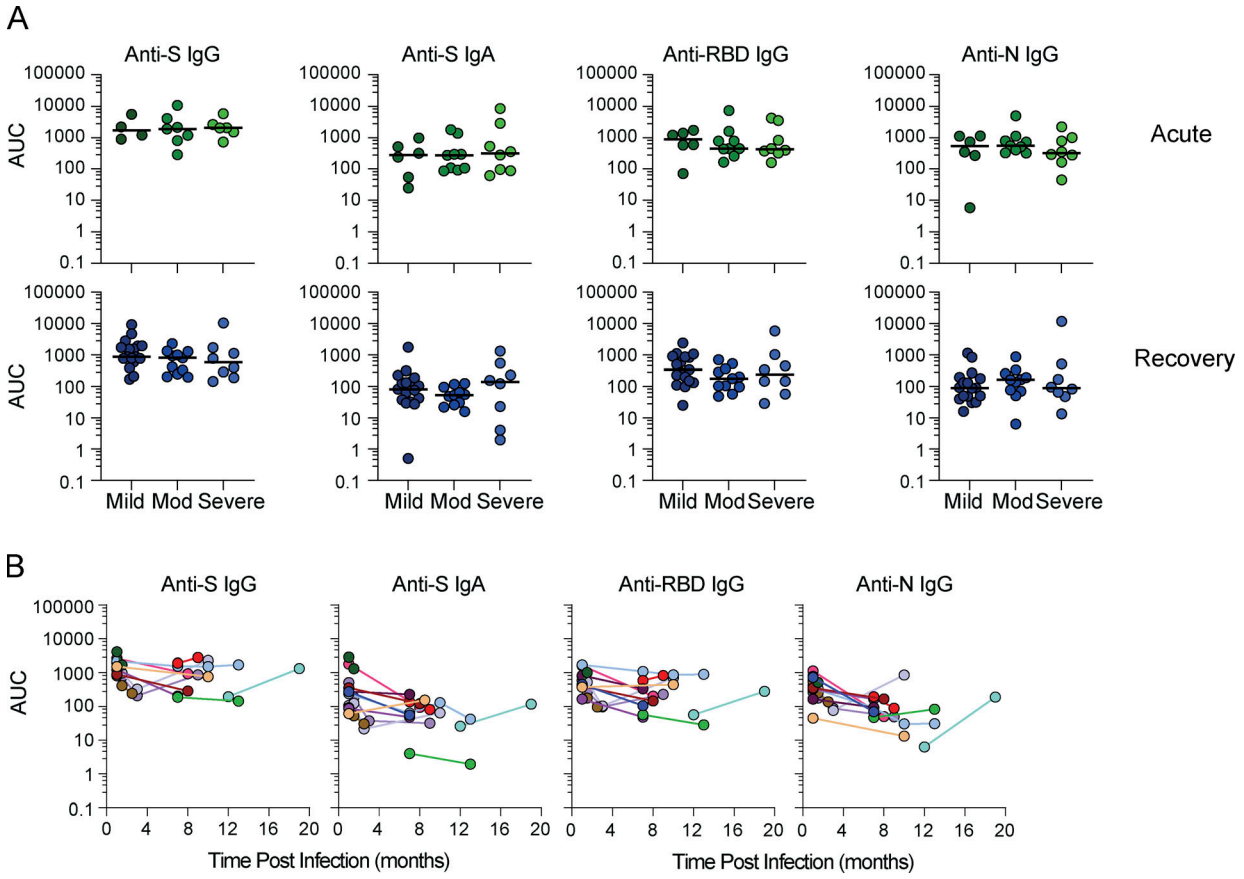

Figure S3. **SARS-CoV-2–specific antibodies in children with MIS-C do not vary by severity of MIS-C and are maintained in recovery. (A)** SARS-CoV-2 antibody reactivity in children with MIS-C stratified by clinical severity during acute (top; mild, *n* = 4–6; moderate, *n* = 7–9; severe, *n* = 6–8) and following recovery (bottom; mild, *n* = 17; moderate, *n* = 11; severe, *n* = 8). Lines depict median. Statistical testing performed using Kruskal–Wallis test. **(B)** Longitudinal visualization of SARS-CoV-2–specific antibodies in children with MIS-C (*n* = 12). Color coordinated lines and dots depict individual MIS-C subjects. *, P < 0.05; **, P < 0.01; ***, P < 0.001; ****, P < 0.0001. Mod, moderate.

Provided online are Table S1, Table S2, Table S3, Table S4, Table S5, Table S6, and Table S7. Table S1 lists CD4⁺ T cell differentially expressed genes. Table S2 lists CD8⁺ T cell differentially expressed genes. Table S3 lists T cell receptor metadata. Table S4 shows multivariate analysis for anti-SARS-CoV-2 AIM assay. Table S5 shows multivariate analysis for anti-SARS-CoV-2 antibody measurements in this study. Table S6 shows multivariate analysis for neutralization activity measurements in this study. Table S7 lists antibodies used for flow cytometry in this study.